

ADA 035460

BRL CR 327

**BRL**

12

*[Handwritten mark]*

AD

CONTRACT REPORT NO. 327

MODEL ANALYSIS FOR PENETRATION OF  
SPACED ARMOR

Prepared by

Southwest Research Institute  
P. O. Drawer 28510  
San Antonio, TX 78284

DDC  
RECEIVED  
FEB 10 1977  
UNLIMITED  
C

January 1977

Approved for public release; distribution unlimited.

USA BALLISTIC RESEARCH LABORATORIES  
ABERDEEN PROVING GROUND, MARYLAND

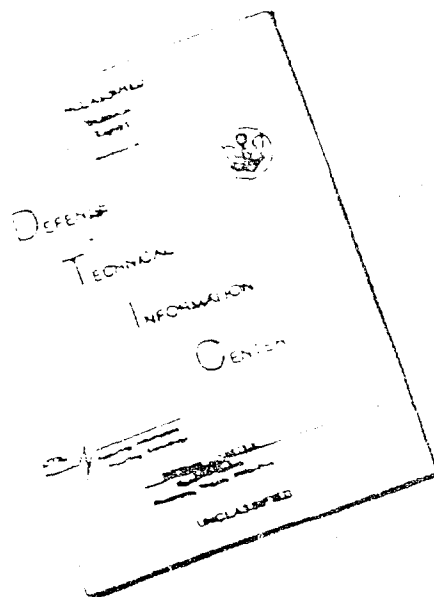
Destroy this report when it is no longer needed.  
Do not return it to the originator.

Secondary distribution of this report by originating  
or sponsoring activity is prohibited.

Additional copies of this report may be obtained  
from the National Technical Information Service,  
U.S. Department of Commerce, Springfield, Virginia  
22151.

The findings in this report are not to be construed as  
an official Department of the Army position, unless  
so designated by other authorized documents.

# DISCLAIMER NOTICE



THIS DOCUMENT IS BEST  
QUALITY AVAILABLE. THE COPY  
FURNISHED TO DTIC CONTAINED  
A SIGNIFICANT NUMBER OF  
PAGES WHICH DO NOT  
REPRODUCE LEGIBLY.

REPRODUCED FROM  
BEST AVAILABLE COPY

UNCLASSIFIED

SECURITY CLASSIFICATION OF THIS PAGE (When Data Entered)

REPORT DOCUMENTATION PAGE (19)		READ INSTRUCTIONS BEFORE COMPLETING FORM
1. REPORT NUMBER BRL CONTRACT REPORT NO. 327	2. GOVT ACCESSION NO. BRL(CR-327)	3. RECIPIENT'S CATALOG NUMBER
4. TITLE (and Subtitle) MODEL ANALYSIS FOR PENETRATION OF SPACED ARMOR	5. TYPE OF REPORT & PERIOD COVERED Final Report. Jun 1975 - Feb 1976	
7. AUTHOR(s) W. E. Baker P. S. Westine	6. PERFORMING ORG. REPORT NUMBER SwRI - 02-4281	8. CONTRACT OR GRANT NUMBER(s) DAAD05-75-C-0757
9. PERFORMING ORGANIZATION NAME AND ADDRESS Southwest Research Institute P. O. Drawer 28510 San Antonio, TX 78284	10. PROGRAM ELEMENT, PROJECT, TASK AREA & WORK UNIT NUMBERS 12 54 P.	
11. CONTROLLING OFFICE NAME AND ADDRESS US Army Ballistic Research Laboratory Aberdeen Proving Ground, MD 21005	12. REPORT DATE JAN 1977	13. NUMBER OF PAGES 55
14. MONITORING AGENCY NAME & ADDRESS (if different from Controlling Office) US Army Materiel Development & Readiness Command 5001 Eisenhower Avenue Alexandria, VA 22333	15. SECURITY CLASS. (of this report) UNCLASSIFIED	
16. DISTRIBUTION STATEMENT (of this Report) Approved for public release; distribution unlimited.		
17. DISTRIBUTION STATEMENT (of the abstract entered in Block 20, if different from Report)		
18. SUPPLEMENTARY NOTES		
19. KEY WORDS (Continue on reverse side if necessary and identify by block number) Scale modeling                      Dissimilar material modeling Spaced armor                        Similitude Rod penetrators                      Dynamic material properties Kinetic energy penetrators        Constitutive similarity Replica modeling                    Dimensional analysis		
20. ABSTRACT (Continue on reverse side if necessary and identify by block number) This report includes a discussion and similitude analysis of the penetration of spaced armor by dense, long rod projectiles. Many geometric and physical parameters are included in the analysis. A general scale model law is given, and the implications of replica and dissimilar material assumptions are discussed in detail. Very few scaling parameters are distorted for either assumption. A model validation test program is recommended for both the replica and dissimilar material assumptions. Practical lower limits on model scale and statistical methods for comparing model and prototype data are briefly discussed.		



TABLE OF CONTENTS

	<u>Page</u>
LIST OF ILLUSTRATIONS	vii
LIST OF TABLES	ix
I. INTRODUCTION	1
II. BACKGROUND	3
III. MODEL ANALYSIS	14
A. Choice of Physical Parameters	14
B. Model Analysis	25
C. Implications of "Replica" Modeling	29
D. Implications of Dissimilar Material Modeling	33
IV. DISCUSSION	38
V. RECOMMENDATIONS	44
REFERENCES	46
DISTRIBUTION LIST	49

## LIST OF ILLUSTRATIONS

<u>Figure</u>		<u>Page</u>
1	Logarithmic Plot of Specific Limit Energy Vs Plate Thickness; Normal Impact, BHN 255 Armor	5
2	Ballistic Limit Curve for Armor Piercing Capped Projectiles Vs Rolled Homogeneous Armor, 30° Obliquity	7
3	Projectile Penetrating Target	8
4	Impact Geometry	15
5	True Yield Stresses at Various Strains Vs Strain Rate for Mild Steel at Room Temperature	18
6	Effect of Strain Rate on Ultimate Stress of Aluminum (1100-0) at Various Temperatures	18
7	Yield Stress Vs Strain Rate for 4340 Fine Grained, Martensite Steel	19
8	Yield Stress Vs Strain Rate for Aluminum Alloy 7075-T6	20
9	Scaled Hugoniot Parameters ( $U/c_0$ ) Vs ( $u/c_0$ ) for Various Materials	22
10	Stress-Strain Curves for Materials Possessing Constitutive Similarity	34
11	Comparison of Single and Triple Target Tests	41

LIST OF TABLES

<u>Table</u>		<u>Page</u>
1	List of Parameters for Projectile Impact-- Transitional Region	9
2	Pi Terms--Projectile Impact in the Transitional Region	10
3	Replica Modeling Law in Transition Range	12
4	Pi Terms--High Velocity Impacts	12
5	Thermal Properties for Model Analysis	23
6	List of Parameters	26
7	List of Pi Terms	28
8	List of Scale Factors for Replica Model	32
9	List of Scale Factors for Dissimilar Material Modeling	35
10	Some Properties of Metals	37

## I. INTRODUCTION

A need exists for improved capability to predict the performance of vehicle armor attacked by kinetic energy projectiles. To this end, the Ballistic Research Laboratories (BRL) have been engaged in experimental work, including a large number of test firings under the Vehicle Armor Technology Project. Full scale firings of anti-tank rounds are extremely costly compared to small-caliber firings, so scaled-down firings present the possibility of great savings. The detailed analysis involved in modeling the perforation of multiple plate targets, including back-face spall and projectile breakup, has not been attempted, and no sub-scale experiments have been performed to date to ascertain the range of validity of scaling laws so derived.

To study problems of scaling and experimental design related to high velocity impact of kinetic energy projectiles against multiple plate targets, BRL has contracted with SwRI. The objectives of this contract are to derive scaling relationships and design experiments to demonstrate whether or not modeling methods will permit prediction of terminal ballistics effects in prototype firings of high length-to-diameter ratio (10/1 to 20/1) rods of two types of projectile materials against oblique, parallel, spaced steel armor targets, based on experimental data from similar models at different scales. This report presents the results of the study.

The prototype (full-scale) conditions which are to be modeled are typified by the penetration of long rods into spaced steel armor targets at ordnance velocities up to 1830 m/s (6000 ft/sec) at various obliquities and various combinations of armor thicknesses and spacing. A typical projectile geometry is a right circular cylinder with a hemispherical nose having length-to-diameter (L/D) ratio between 10 and 20 and a mass of 3 kg. It can have an attached windscreen of a different material and fins of a different material. Projectile penetrator materials are materials of high density and high strength, such as a heat treated tool steel, a heat treated uranium alloy, or a sintered tungsten alloy. Prototype targets usually consist of parallel, spaced arrays of flat steel armor plates of high strength, high elongation alloys. The armor material may either be essentially homogeneous and isotropic or have significant inhomogeneity and anisotropy.

For the types of projectiles, targets, and impact conditions considered in this study, a large number of physical, material and geometric parameters are needed to completely characterize the processes of interaction of projectile and target. In general, both target and projectile erode, deform elastically and plastically, and/or break up. In at least part of the penetration process, both projectile and target materials are subjected to stresses far exceeding yield and behave hydrodynamically. Intense plastic or elastic waves are generated in

penetrator and target, and gross deformations and breakup can occur during the penetration of successive plates in the spaced armor targets. Many more geometric parameters are needed to define impact conditions for these relatively complex projectiles and targets than for armor-piercing projectiles of older design versus monolithic armor. These and other parameters are considered in the model analysis.

A basic question in experimental validation of any physical theory of penetration and breakup, or in validation of a model analysis and inferences drawn from the analysis, is, "How can I prove the theory or model analysis by experiment?" To answer this question, one must invoke statistical methods because there is always scatter or variation in the results of experiments, whatever the scale of the experiments. As applied to modeling projectile penetration, an example is the experimental determination of curves of striking velocity versus limit velocity.\*

A model law can usually be phrased as a prediction that some dimensionless parameter related to striking velocity determines another dimensionless parameter related to limit velocity, provided a host of still other dimensionless parameters are held constant. Statistical testing of appropriately scaled model and prototype test data can be used to validate the model law or determine the range of scaled parameters over which it is valid. Such statistical methods of comparison are discussed in this report.

The following section presents the background of this problem and covers past work in modeling in penetration mechanics. Then, in Section III we give a thorough model analysis of the problem outlined in this section, an extended discussion of physical parameters chosen as significant, and of the implications of the similarity (model) analyses.

Section IV covers a discussion of the results of the model analysis and statistical techniques. Design of experiments which we believe necessary to test the model law or laws is covered in Section V. A list of references completes the report.

---

\* Limit velocity is the velocity for threshold of complete penetration of armor by a projectile.

## II. BACKGROUND

Studies of penetration mechanics, both experimental and theoretical, are numerous and ancient. They cover a wide spectrum of types of penetrator, impact conditions, and targets. Penetrators can be jagged fragments, cubes, spheres, "conventional" cylindrical projectiles with L/D ratios of 3 or less and various nose shapes, or slender projectiles of L/D greater than 10. Impact velocities can range from less than 100 m/s to over 1500 m/s, depending on type of penetrator and target. Targets can be very "soft" (human beings or thin sheet metal), of medium "hardness" (earthworks or reinforced concrete bunkers), or very "hard" (monolithic or spaced tank armor). Because the physical processes governing penetration for almost any combination of penetrator and target are very complex, most theoretical and many experimental studies are limited to specific penetrator-target combinations and velocity regimes. The state of the art of even the most sophisticated computer programs for prediction of high velocity penetration is still limited to axisymmetric projectiles impacting monolithic targets at normal obliquity.<sup>1,2</sup>

Because accurate theoretical studies are difficult, most of penetration mechanics is based on experiment. The number of terminal ballistic tests conducted over the years, with different combinations of projectiles, impact conditions, and targets is probably beyond counting--and they still continue as "new" combinations are conceived and tested by ordnance specialists. Many of these tests have been conducted full scale, at great expense in money and time, for large caliber projectiles. All too often, the tools of model analysis have been ignored in comparing tests at different calibers, or as a design tool to predict performance by sub-scale testing prior to full-scale testing.

There appears to have been little application of scaling principles to penetration mechanics prior to World War II. But, terminal ballistic studies of penetrations into steel plate and reinforced concrete slabs sponsored by National Defense Research Council (NDRC) during that war were obviously guided by scaling considerations. Curtis<sup>3</sup> stated that dimensional analysis indicated perforation formulas for armor-piercing projectiles against plate should have the alternate forms:

$$\frac{e_1}{d^3} = \bar{c} f \left( \frac{t}{d}, \theta \right) \quad (1a)$$

or

$$\frac{W v_\ell^2}{d^3} = c f \left( \frac{t}{d}, \theta \right) \quad (1b)$$

where

$$c = 2 g \bar{c}$$

In these equations,

- $e_1$  = limit energy = minimum energy required for perforation
- $W$  = projectile weight
- $V_l$  = limit velocity
- $d$  = maximum projectile diameter (caliber)
- $t$  = plate thickness
- $\bar{c}$  = measure of strength of plate material expressed as force per unit area
- $g$  = acceleration due to gravity
- $f\left(\frac{t}{d}, \theta\right)$  = a general function of  $\frac{t}{d}$  and  $\theta$
- $\theta$  = angle of incidence

Curtis called the parameter  $(WV_l^2/d^3)$  the specific limit energy. His analysis was limited to non-deforming projectiles, and it therefore included no strength properties of the projectile. An empirical plot from Reference 3 shows some data for small caliber projectiles fired versus various scaled thickness of armor (Figure 1). Curtis notes that there is a minor "scale effect," i.e., a contradiction to Eq. (1), with a slight tendency for specific limit energy to decrease as projectile caliber increases. He suggests that this deviation from scaling may be connected with the occurrence of inclusions in the armor. He discounts strain rate effects and differences in basic strength properties of thick and thin plates as explanations of the "scale effect."

Following the World War II work, it apparently became common practice to report penetration and perforation data for armor-piercing projectiles in terms of projectile calibers, as typified by an extensive compilation by Killian.<sup>4</sup> Separate plots are provided in Reference 4 for each type of projectile and impact obliquity, for homologous projectiles. Killian defines homologous projectiles as ones with weights varying as the third power of their diameters and lengths varying as the first power of their diameters. He apparently tacitly assumes nose shapes to be similar. (We would use the term "geometrically similar"

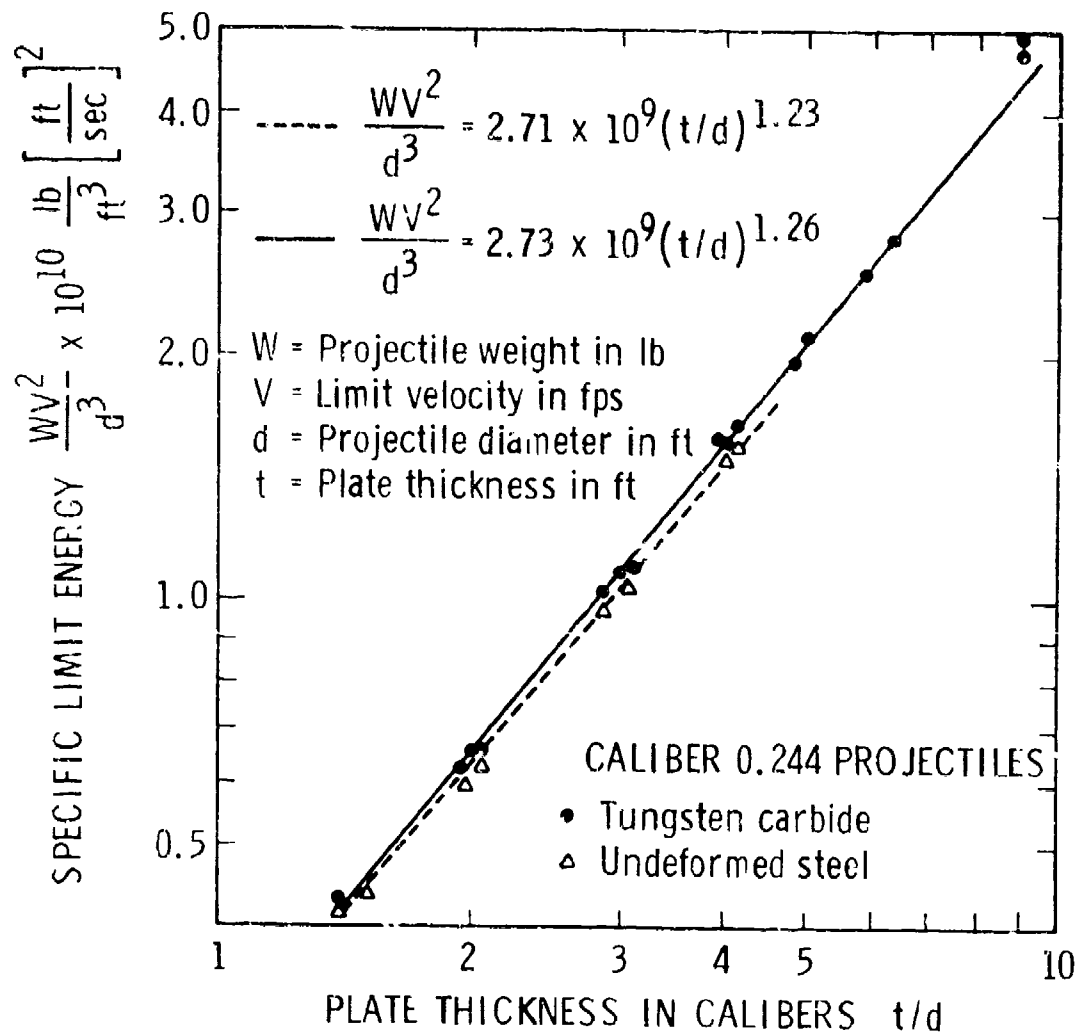


FIGURE 1. LOGARITHMIC PLOT OF SPECIFIC LIMIT ENERGY  
 VS PLATE THICKNESS; NORMAL IMPACT,  
 BHN 255 ARMOR(3)

rather than "homologous" in this context because homology can apply to variables other than geometric ones.) A typical plot from Reference 4 is shown in Figure 2. The abscissa is identical to that in Figure 1, but the ordinate is now simply the limit velocity, which can be obtained from the term  $(WV_0^2/d^3)$  under the assumption that  $W$  is proportional to  $d^3$  and by taking the square root.

A rather comprehensive discussion of modeling in penetration mechanics is given by Baker, Westine and Dodge in Chapter 8 of Reference 5. These authors use the definition of regions of impact of Summers and Charters,<sup>6</sup> as follows:

- (1) Low velocity region - undeformed projectile,
- (2) Transition region - significant to great projectile deformation,
- (3) Fluid impact region - projectile completely melted and/or vaporized.

They then present model analyses for projectile impacts as typified by the geometry and properties of Figure 3, for all three impact regions. As an example, Table 1 is a list of physical parameters which were considered important in the transitional region, and Table 2 is a resulting set of dimensionless parameters from the model analysis. Term  $\pi_{14}$  is the dimensionless equivalent of a limit velocity, while term  $\pi_{15}$  is the projectile penetration or perforation in calibers. A number of constitutive properties for both projectile and target enter the similitude analysis, and these in turn appear in many  $\pi$  terms in Table 2. A type of shorthand notation is also used in terms such as  $\sigma_1$  and  $S_1$ , implying ratios of components of stress tensors to a basic quantity with dimensions of stress. This in turn implies complete constitutive similarity. By contrast, Curtis's model law in Eq. (1a) or (1b) includes a single constitutive property for the target material, so that his parameter  $\bar{C}$  is probably the counterpart of  $S$  in the analysis of Baker, et al.<sup>5</sup> Note also that projectile weight  $W$  and acceleration of gravity  $g$  do not appear explicitly in Table 1 or Table 2. Instead, enough geometric parameters are included to completely define projectile volume, and projectile density is also listed. The projectile mass  $M$  is scaled in Table 2, where\*

---

\*The insertion of  $g$  by Curtis in Eq. (1b) introduces a parameter which should not enter this scaling law. Projectile mass is important in this problem, not weight, and the acceleration of gravity has no bearing on this problem.

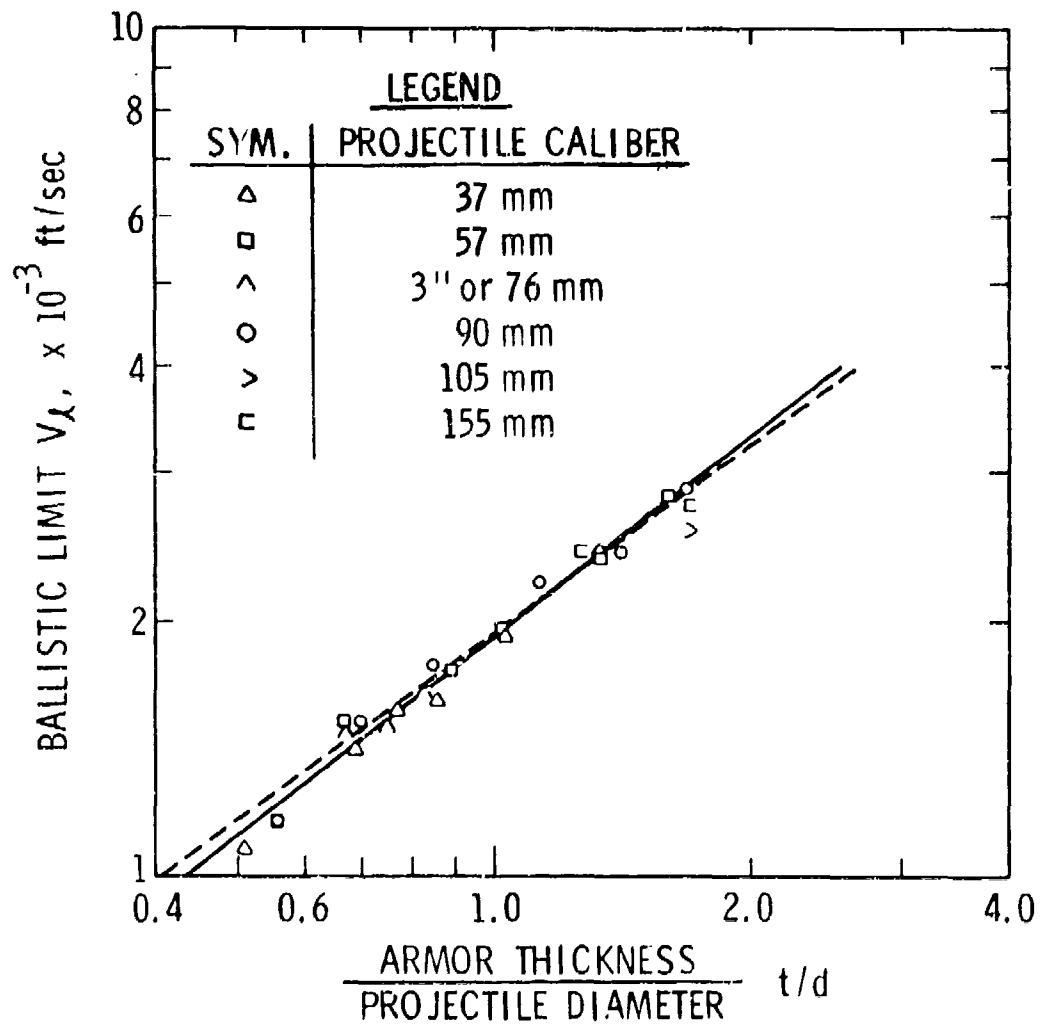


FIGURE 2. BALLISTIC LIMIT CURVE FOR ARMOR PIERCING CAPPED PROJECTILES VS ROLLED HOMOGENEOUS ARMOR, 30° OBLIQUITY (Fig. 14A of Ref. 6)

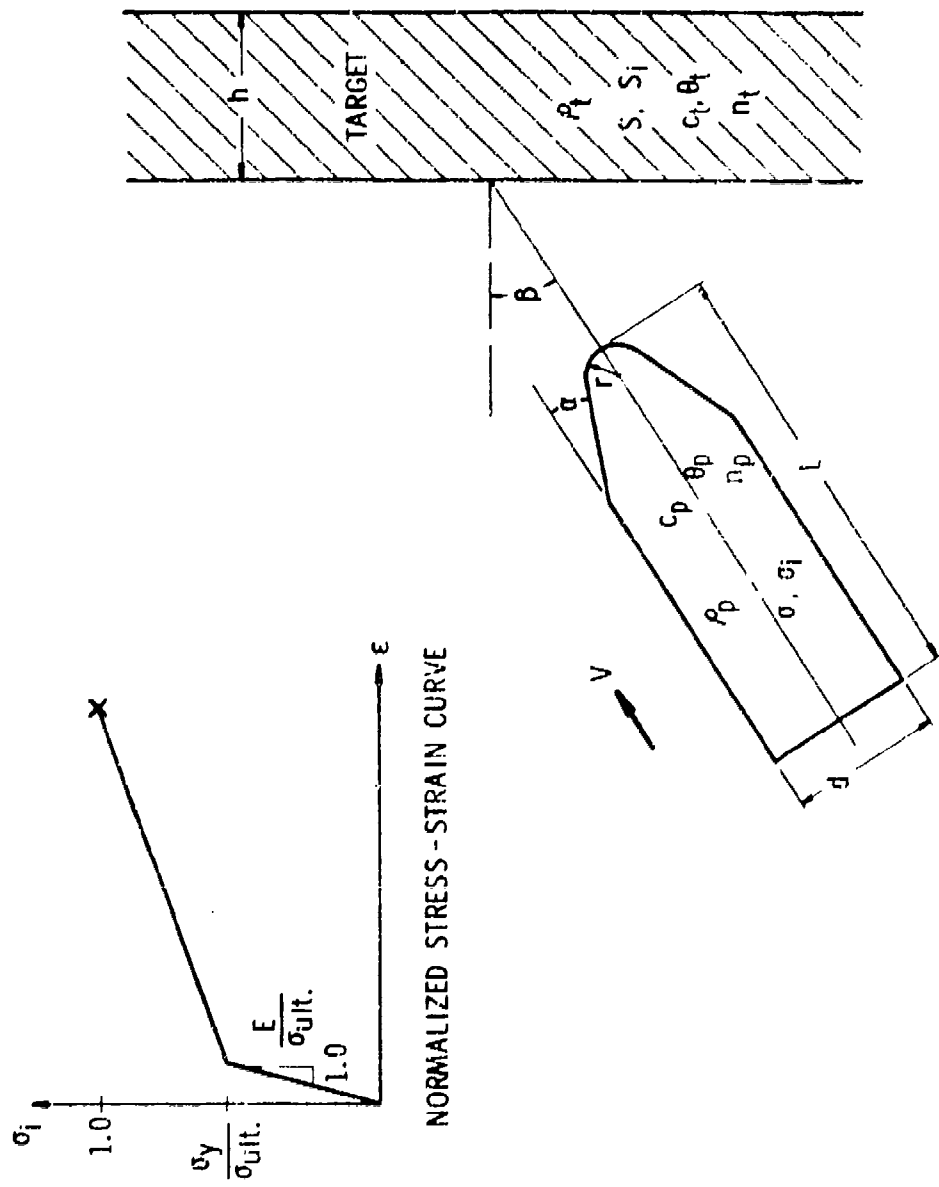


FIGURE 3. PROJECTILE PENETRATING TARGET (5)

TABLE I. LIST OF PARAMETERS FOR PROJECTILE IMPACT--  
TRANSITIONAL REGION<sup>(5)</sup>

<u>Variable</u>	<u>Symbol</u>	<u>Fundamental Dimensions</u>
Caliber of bullet	d	L
Length of bullet	L	L
Nose radius of projectile	r	L
Angle of projectile nose	$\alpha$	-
Angle of obliquity	$\beta$	-
Density of projectile	$\rho_p$	$FT^2/L^4$
Velocity of projectile	V	L/T
Thickness of target	h	L
Density of target	$\rho_t$	$FT^2/L^4$
Temperature of target	$\theta_t$	$\theta$
Specific heat of target	$c_t$	$L^2/\theta T^2$
Heat of fusion of target	$n_t$	$L^2/T^2$
Temperature of projectile	$\theta_p$	$\theta$
Specific heat of projectile	$c_p$	$L^2/\theta T^2$
Heat of fusion of projectile	$n_p$	$L^2/T^2$
Ultimate stress of target	S	$F/L^2$
Ultimate stress of projectile	$\sigma$	$F/L^2$
Other stress or strength rates of target	$S_i$	$F/L^2$
Other stress or strength rates of projectile	$\sigma_i$	$F/L^2$
Strain	$\epsilon$	-

TABLE 2. PI TERMS--PROJECTILE IMPACT IN THE  
TRANSITIONAL REGION<sup>(5)</sup>

$\pi_1$	=	$\alpha$	}	Geometric similarity
$\pi_2$	=	$\beta$		
$\pi_3$	=	$L/d$		
$\pi_4$	=	$r/d$		
$\pi_5$	=	$h/d$		
$\pi_6$	=	$\rho_p/\rho_t$		Similar density ratios
$\pi_7$	=	$\epsilon$	}	Constitutive similarity
$\pi_8$	=	$\sigma/S$		
$\pi_9$	=	$S_i/S$		
$\pi_{10}$	=	$\sigma_i/S$		
$\pi_{11}$	=	$\theta_p/\theta_t$		Similar temperature
$\pi_{12}$	=	$n_p/n_t$		Similar heats of fusion
$\pi_{13}$	=	$c_p/c_t$		Similar specific heats
$\pi_{14}$	=	$\rho_t^{1/2} v/S^{1/2}$	}	Energy ratios
$\pi_{15}$	=	$\rho_t \theta_t c_t/S$		
$\pi_{16}$	=	$\rho_t n_t/S$		

$$M = \frac{W}{g} \quad (2)$$

Baker, et al.,<sup>5</sup> note that a replica model law is consistent with Table 2, implying that all material properties must be kept identical and all geometries must be scaled by the geometric scale factor in model and prototype. If this is done, scale factors for all physical parameters in Table 1 are as shown in Table 3.

Baker, et al.,<sup>5</sup> note that the law given by Table 2 is a rather general one and includes model laws for the low velocity region and the high velocity fluid impact region as special cases. In the high velocity region, they note that alternate forms of the last three pi terms in Table 2 are

$$\left. \begin{aligned} \pi_{14-a} &= \frac{v^2}{n_t} \\ \pi_{15-a} &= \frac{\theta_i c_t}{n_t} \\ \pi_{16-a} &= \frac{S}{\rho_t n_t} \end{aligned} \right\} \quad (3)$$

and that  $\pi_{15-a}$  is essentially a constant for all metals, and so can be dropped from the analysis. The  $S_i$ ,  $\sigma_i$  and  $S/\rho_t n_t$  are dropped from the general solution because mechanical strength is unimportant for high velocity impacts. This procedure gives Table 4.

Subsequently, it is demonstrated that  $c_t \theta_i / n_t$  is almost constant for most metals, making  $\pi_{15-a}$  no problem. Finally, data are used to show  $V^2/n_t$  is  $V^2/a^2$ , or the square of the Mach Number. Data from the literature are given in Reference 5 to show the validity of this law. The authors of Reference 5 also show that many of the low velocity empirical penetration equations available in the literature are of the form

$$\frac{\rho_t^{1/2} V}{S^{1/2}} = f \left( \text{geometric similarity, } \frac{S}{\sigma}, \frac{\rho_p}{\rho_t} \right) \quad (4)$$

As an example, the left hand side of Eq. (1b) can be written

TABLE 3. REPLICA MODELING LAW IN  
TRANSITION RANGE<sup>(5)</sup>

<u>Variable</u>	<u>Symbol</u>	<u>Scale Factor</u>
Geometric lengths	$d, L, r, h$	$\lambda$
Angles	$\alpha, \beta$	1.0
Stress	$\sigma, S$	1.0
Strain	$\epsilon$	1.0
Density	$\rho_t, \rho_p$	1.0
Velocity	$v$	1.0
Temperature	$\theta_t, \theta_p$	1.0
Specific heats	$c_t, c_p$	1.0
Heats of fusion	$n_t, n_p$	1.0

TABLE 4. PI TERMS--HIGH VELOCITY IMPACTS

$\pi_1$	=	$\alpha$	} Geometric similarity
$\pi_2$	=	$\beta$	
$\pi_3$	=	$L/d$	
$\pi_4$	=	$r/d$	
$\pi_5$	=	$h/d$	
$\pi_6$	=	$\rho_p/\rho_t$	Similar density ratios
$\pi_{11}$	=	$\theta_p/\theta_t$	Similar temperatures
$\pi_{12}$	=	$n_p/n_t$	Similar heats of fusion
$\pi_{13}$	=	$c_p/c_t$	Similar specific heats
$\pi_{14-a}$	=	$v^2/n_t$	Normalized velocity of impact
$\pi_{15-a}$	=	$\theta_t c_t/n_t$	Energy to raise temperature of metal relative to energy to cause liquefaction

$$\frac{WV_l^2}{d^3 2gc} = \frac{MV_l^2}{d^3 2c} \sim \frac{\rho_t d^3 V_l^2}{d^3 S} = \frac{\rho_t V_l^2}{S} \quad (5)$$

This is the square of the left hand side of Eq. (4).

References on scaling of penetration mechanics in the transition and fluid impact regions, other than the few cited in Reference 5, are scarce. Dienes and Walsh<sup>7</sup> use dimensional analysis to reduce the set of differential equations governing hypervelocity impact phenomena to a smaller set before computer solution. Some data on small-scale Bearcat<sup>®</sup>\* steel penetrators with (L/D) = 10 against single and triple aluminum plate targets are reported by Wenzel and Hokanson,<sup>8</sup> but no model prototype comparisons are made.

---

\* Bearcat is a registered trademark of Bethlehem Steel Corporation for their patented formulation of AISI-S7 tool steel.

### III. MODEL ANALYSIS

#### A. Choice of Physical Parameters

In conducting a model analysis of the penetration of spaced armor by long rod penetrators, the first (and probably most important) step is the choice of physical parameters which are felt to be important, and the listing of their dimensions. Because the penetrator and target are both of complex geometry and because the impacts are occurring in the fluid flow and transition regions discussed earlier, a large number of physical and geometric parameters are needed to characterize the problem. Rather than simply listing the parameters we feel are important, we present here our rationale for inclusion or omission of each property or group of properties. (To keep the number of parameters within bounds for this complex problem, we will freely employ the shorthand notation of a symbol with a subscript "i" for similar physical quantities having the same dimensions.) The fundamental dimensions used for the various quantities are force (F), length (L), time (T), and temperature ( $\theta$ ). We could just as easily and accurately use mass (M) in place of force, but the (F, L, T,  $\theta$ ) set of dimensions will suffice.\*

Let us first cover those quantities which describe the geometry of the problem. Figure 4 shows the geometry of a typical long rod projectile just prior to impact on spaced armor. Let "d" mean "dimensionally equal" or "has the dimensions of," and (-) mean "dimensionless"; then the projectile is impacting with a striking velocity  $V_s \stackrel{d}{=} (L/T)$ , whose direction makes an angle  $\beta \stackrel{d}{=} (-)$  to the surface of the first plate in the plane containing the target normal and velocity vector. The projectile flies at some yaw angle component  $\delta_1 \stackrel{d}{=} (-)$  in this plane (pitch) and some yaw angle component normal to this plane,  $\delta_2 \stackrel{d}{=} (-)$ , with respect to the impact angle  $\beta$ . Definition of projectile geometry requires a large number of lengths  $l_i \stackrel{d}{=} (L)$  and angles  $\alpha_i \stackrel{d}{=} (-)$ , some of which are shown schematically in Figure 4. We also choose the diameter d (or caliber) of the main body of the finned projectile as a particular characteristic length. The geometry of the target, which consists of parallel, flat armor plates of various thicknesses and spacings, is fixed by specifying a characteristic thickness h of the first layer, thicknesses of other layers  $h_i$ , and spacings of

\* For reasons which will be discussed later, a dimensional constant such as the mechanical equivalent of heat must appear in the list of parameters when  $\theta$  is listed as a fundamental dimension.

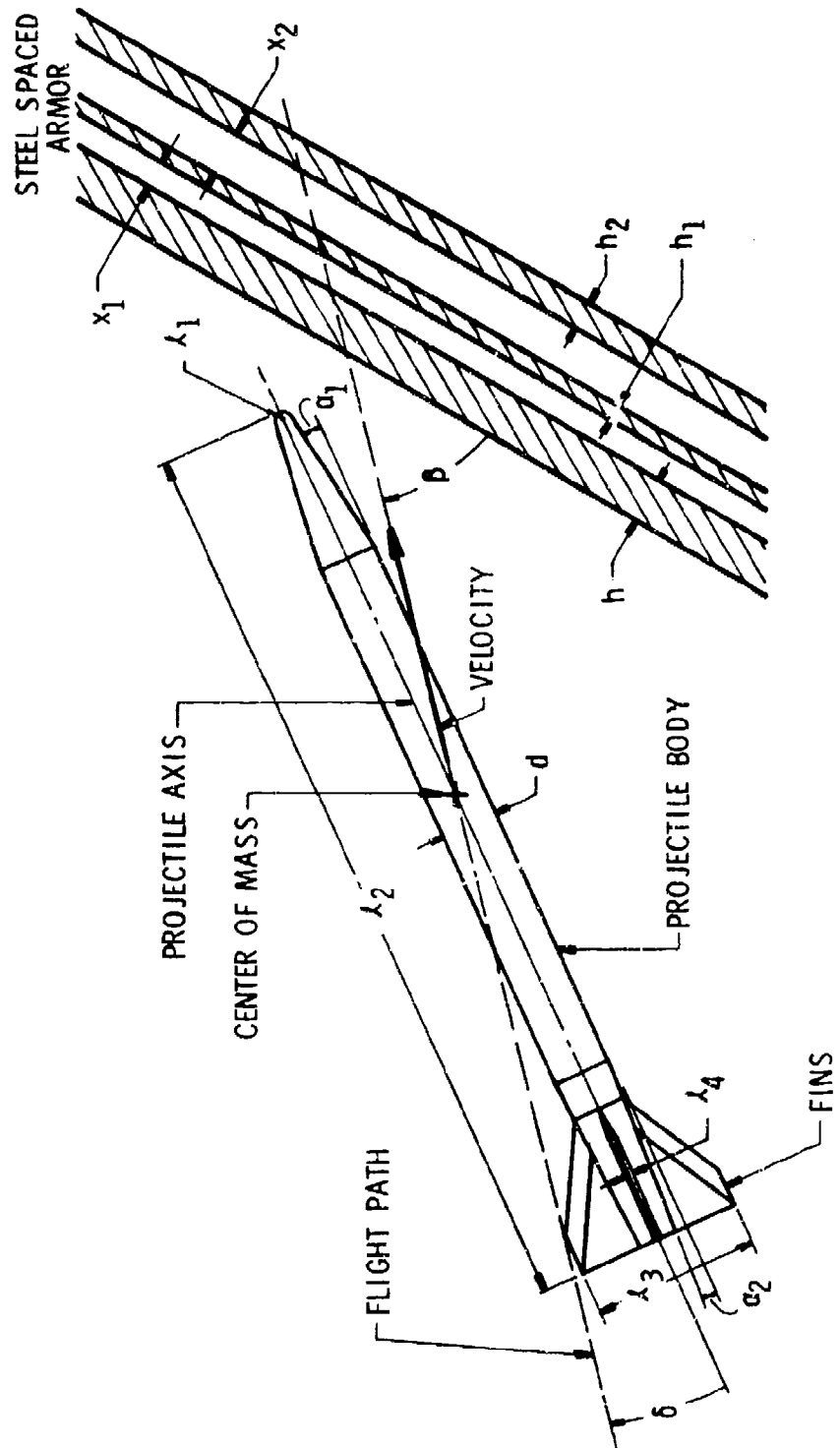


FIGURE 4. IMPACT GEOMETRY

layers  $x_i$ , all with dimensions of length  $L$ . So, we list ten geometric parameters. The important consideration is not the exact number of such parameters which we include, but is instead the inclusion of enough lengths and angles, either explicitly or implicitly by the shorthand subscript, to completely fix the geometry of projectile, target, and impact.

We are also interested in some geometric parameters after impact, and this geometry is almost certain to be very complex because the projectile can break up as it penetrates the spaced armor, and the armor can spall. A number of jagged pieces will be flying about in various directions, and exact description of this geometry does not seem possible. Instead, we assume that enough detail can be given by inclusion of the parameters  $r \stackrel{d}{=} (L)$  for characteristic mean (linear dimension) of projectile or spall particles, number of particles  $N \stackrel{d}{=} (-)$ , distribution functions  $f_i \stackrel{d}{=} (-)$  for sizes or masses of fragments, and  $\gamma_i \stackrel{d}{=} (-)$  for fragment trajectory angles. The actual number of parameters included in  $f_i$  and  $\gamma_i$  may be huge.

Let us next consider material properties. In the model analysis of projectile impact in the transition region<sup>5</sup> discussed in Section II, a number of material properties for both projectile and target were included. We must include at least as many parameters in this analysis and may have to add more. The properties which we feel should be included are:

- (1) Dynamic constitutive properties, including wave transmission properties
- (2) Fracture toughness
- (3) Hugoniot properties
- (4) Other continuum properties
  - (a) Densities
  - (b) Heat capacities
  - (c) Heats of fusion
  - (d) Heats of vaporization
- (5) Microscopic properties
  - (a) Grain size
  - (b) Flaw size
  - (c) General microstructure, expressed as length ratios

Dynamic constitutive properties of metals under triaxial states of stress, high strain rates, and for large plastic deformations up to fracture, are all involved in this problem. Complete definition of these parameters would require a very large number of parameters because nine components of stress tensors and strain tensors are required, as well as yield and rupture criteria involving invariants of stress tensors. But, for the model analysis the real requirement is that stress states and strain states be homologous at homologous locations and times. We can assure this by choosing characteristic yield or failure stresses for projectile material,  $\sigma \stackrel{d}{=} (F/L^2)$ , and for target material,  $S \stackrel{d}{=} (F/L^2)$ , and by also indicating other components of the stress tensors as  $\sigma_{ij} \stackrel{d}{=} (F/L^2)$  and  $S_{ij} \stackrel{d}{=} (F/L^2)$ . Included in these latter parameters by inference are elastic moduli such as Young's modulus, bulk modulus, and shear modulus for each material. Wave transmission velocities are included in both projectile,  $c_p \stackrel{d}{=} (L/T)$ , and target,  $c_t \stackrel{d}{=} (L/T)$ . We complete our specification of dynamic constitutive properties by including in our list of parameters characteristic strains,  $\epsilon_p \stackrel{d}{=} (-)$  and  $\epsilon_t \stackrel{d}{=} (-)$ , and components of the strain tensors,  $\epsilon_{pij} \stackrel{d}{=} (-)$  and  $\epsilon_{tij} \stackrel{d}{=} (-)$ .

In listing dynamic constitutive properties, we have deliberately omitted strain rates. This is done, not because knowledge of these properties at high strain rates is not important in the physics of high velocity penetration,<sup>9</sup> but because strain rates will only differ by at most an order of magnitude between model and prototype experiments.\* Stress-strain curves for many metals are indeed affected markedly when one attempts to compare results at very slow rates to those encountered in high velocity penetration. This is particularly true for low yield, ductile materials. Figures 5 and 6, from Reference 9, indicate dependence of yield stress on strain rate for mild steel and a soft aluminum alloy.

However, high yield alloys, which are much more typical of the materials used in high velocity penetrators and in armor, usually exhibit minimal effect of strain rate on yield or ultimate stress. This is evident in Figure 7 for 4340 steel and Figure 8 for 7075-T6 aluminum alloy, from Reference 10. The yield stress for the high-strength steel increases by only 4% over five decades of strain rates, and the increase for the high-strength aluminum alloy is even less. Even assuming the worst case, for high strain rates for mild steel (Figure 5), the ultimate stress only increases by 10% over the single decade which is the practical upper limit for change in strain rate between our model and

---

\* We will show later that practical model scales for this problem are  $\lambda \geq 1/10$ .

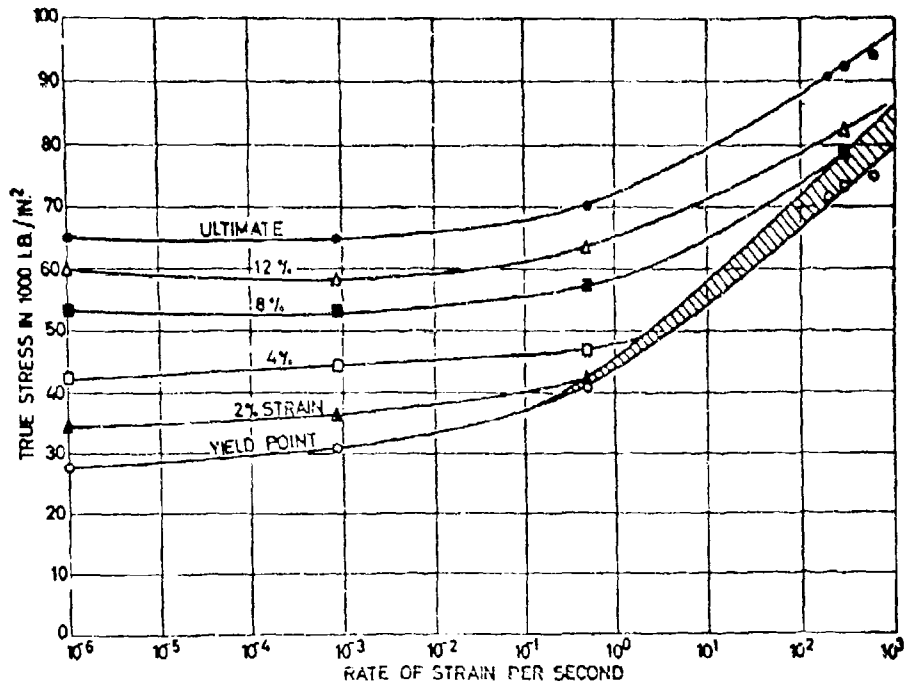


FIGURE 5. TRUE YIELD STRESSES AT VARIOUS STRAINS VS STRAIN RATE FOR MILD STEEL AT ROOM TEMPERATURE(9)

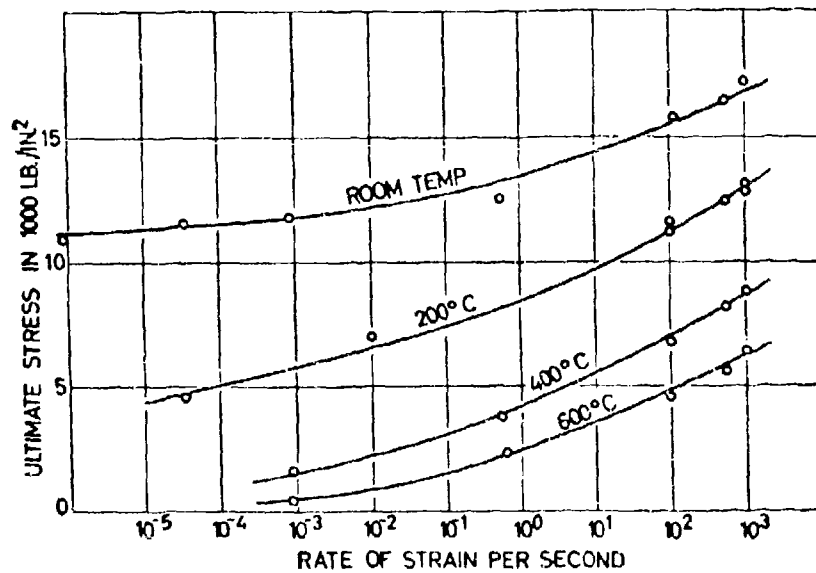


FIGURE 6. EFFECT OF STRAIN RATE ON ULTIMATE STRESS OF ALUMINUM (1100-0) AT VARIOUS TEMPERATURES(9)

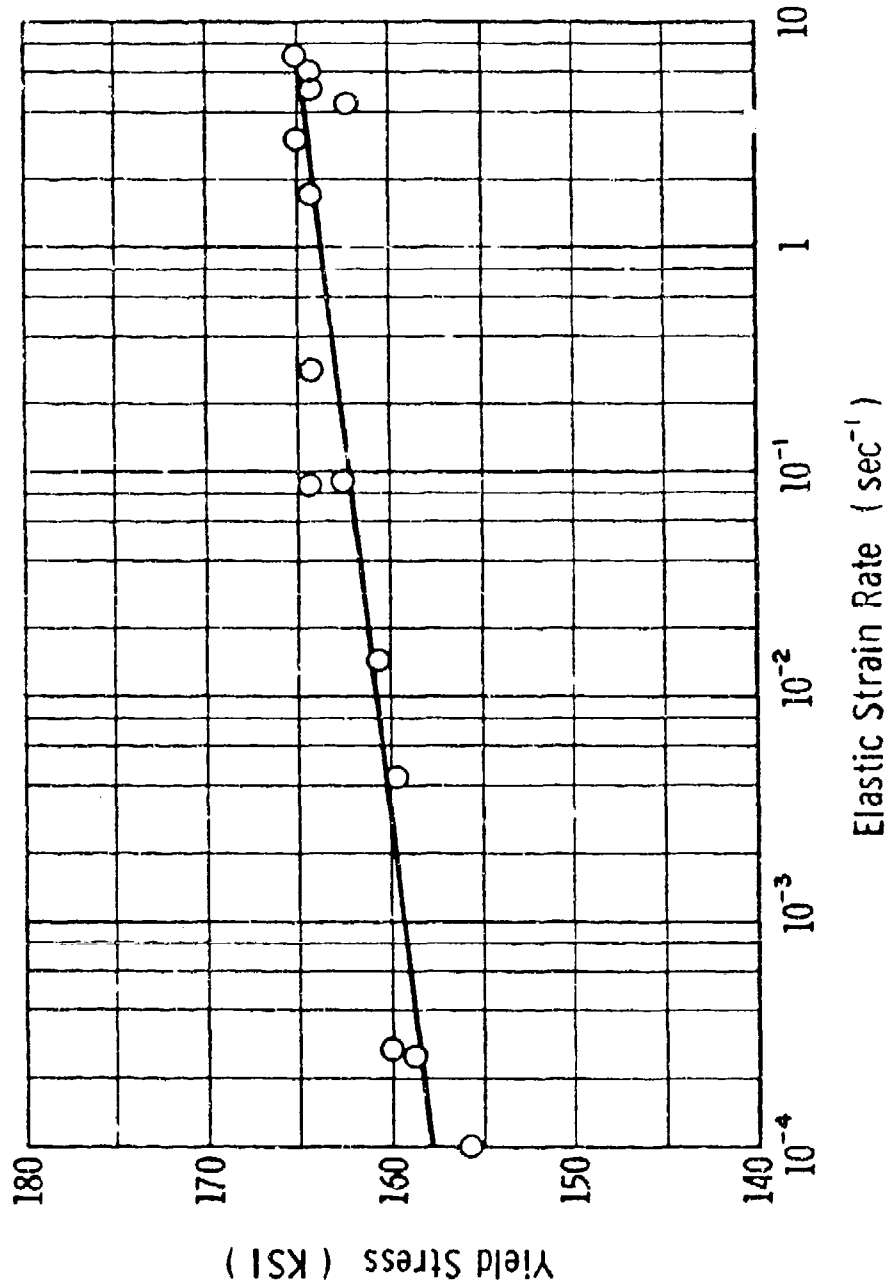


FIGURE 7. YIELD STRESS VS STRAIN RATE FOR 4340 FINE GRAINED, MARTENSITE STEEL (10)

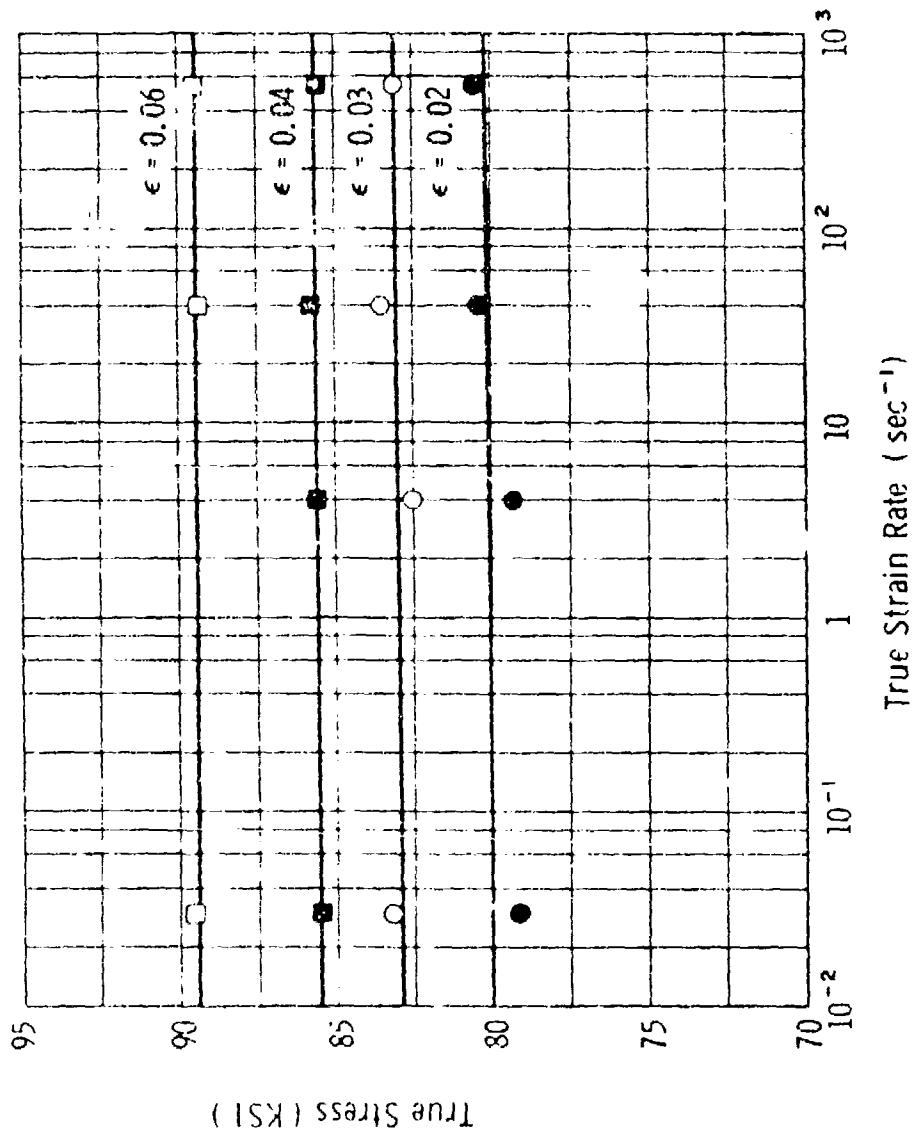


FIGURE 8. YIELD STRESS VS STRAIN RATE FOR ALUMINUM ALLOY 7075-T6

prototype penetration tests. Much more experimental evidence could be cited to reinforce our decision to omit strain rate as a significant parameter in the model analysis, but we believe that this discussion should suffice.

A property which relates to fracture under impact, and which probably involves both basic material properties and some aspects of the tests used to measure the property, is fracture toughness,  $K_c \stackrel{d}{=} (F/L^{3/2})$ . This property should be included in our analysis for both projectile and target materials. It seems quite probable that this quantity is in reality

$$K_c = (\ell_f)^{1/2} (\Delta_f) \quad (6)$$

where  $\ell_f \stackrel{d}{=} (L)$  is the length of a critical flaw in the projectile or target material, and  $\Delta_f \stackrel{d}{=} (F/L^2)$  is fracture energy per unit volume.

The latter quantity is essentially the area under the stress-strain curve for the material and has the dimensions of stress. Although inclusion of these two parameters or the fracture toughness itself will suffice, we choose the latter course.

When the impacts are at high enough velocity that all or part of the material behavior lies in the fluid impact region, the description of dynamic material properties becomes much simpler because the materials behave as compressible, inviscid fluids. They do not support shear, and one need only consider scalar pressures and their relation to shock velocity, particle velocity, or volume change. The resulting Hugoniot relations are completely defined for most metals, including steels, tungsten and uranium alloys, through the empirical relation<sup>11,12</sup>

$$U = c_0 + s u \quad (7)$$

where  $U$  is shock velocity,  $c_0$  is sound velocity,  $s$  is a dimensionless constant ranging between 1.0 and 1.7 for most materials, and  $u$  is particle velocity behind the shock front. If data from Reference 11 and other sources are scaled, one can see that a mean value of  $s$ , say

$$\bar{s} = 1.435 \quad (8)$$

represents a wide variety of materials with little error (Figure 9). We have already included  $c_0$  in our list of parameters, and so need only add  $s \stackrel{d}{=} (-)$  to complete the Hugoniot description.

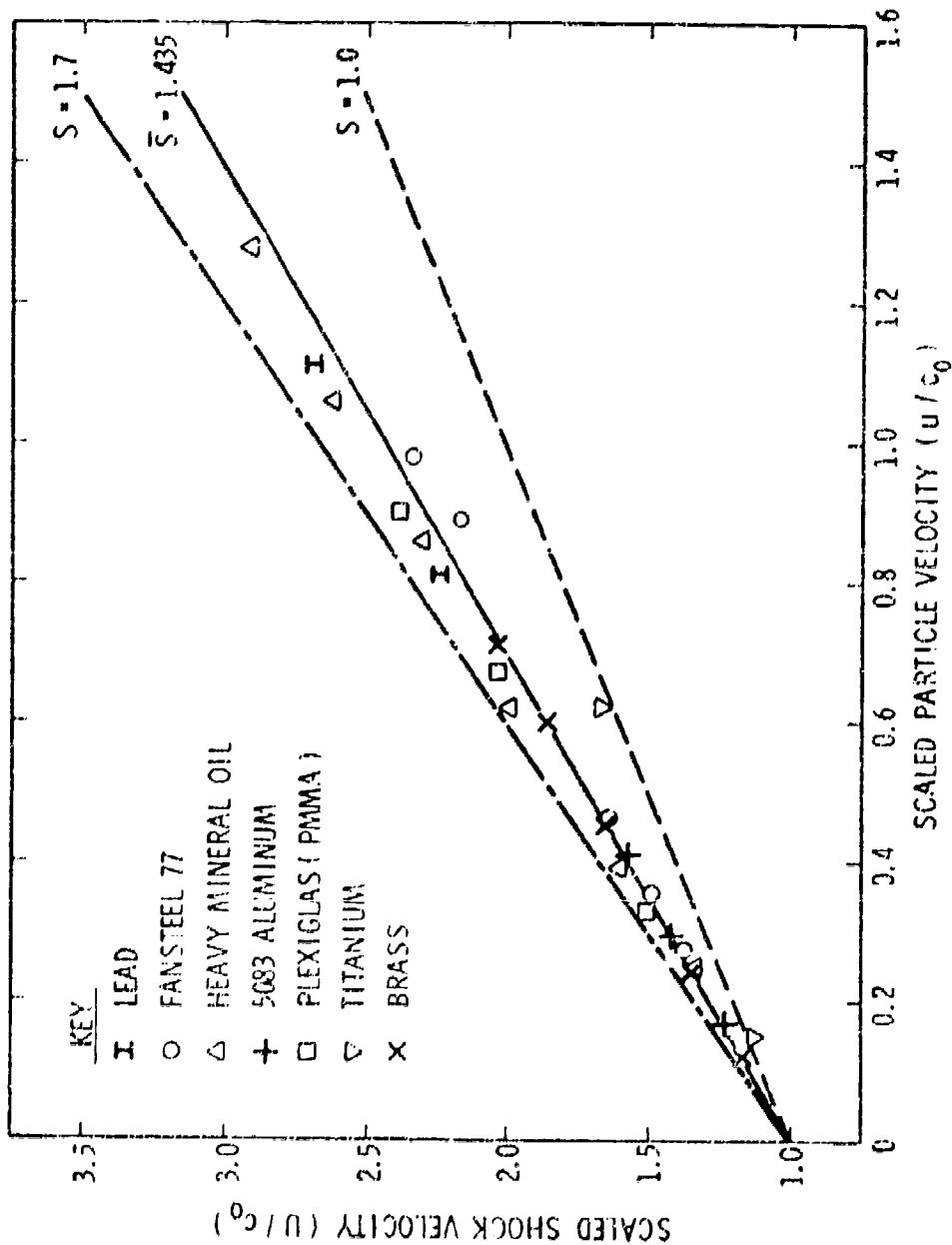


FIGURE 9. SCALED HUGONIOCT PARAMETERS ( $u/c_0$ ) VS ( $u/c_0$ ) FOR VARIOUS PARAMETERS

A number of more mundane continuum or state properties are needed to complete our list of material properties. These are, in general, easily measured or are available from handbooks. They include densities of projectile  $\rho_p \stackrel{d}{=} (FT^2/L^4)$  and target  $\rho_t \stackrel{d}{=} (FT^2/L^4)$ , initial temperatures of projectile  $\theta_p \stackrel{d}{=} (\theta)$  and target  $\theta_t \stackrel{d}{=} (\theta)$ , and melting temperatures of projectile  $\phi_p \stackrel{d}{=} (\theta)$  and target  $\phi_t \stackrel{d}{=} (\theta)$ . A number of thermal or thermodynamic energy parameters must also be included. We choose to include the list in Table 5.

TABLE 5. THERMAL PROPERTIES FOR MODEL ANALYSIS

Specific heat of projectile material	$C_p \stackrel{d}{=} (\theta)$
Heat of fusion for projectile	$n_p \stackrel{d}{=} (L^2/T^2)$
Internal (thermal) energy in target	$E_t \stackrel{d}{=} (L^2/T^2)$
Nondimensional (thermal) material coefficients in target	$a_t \stackrel{d}{=} (-)$
Specific heat of target	$C_t \stackrel{d}{=} (\theta)$
Heat of fusion for target	$n_t \stackrel{d}{=} (L^2/T^2)$
Internal (thermal) energy in projectile	$E_p \stackrel{d}{=} (L^2/T^2)$
Nondimensional (thermal) material coefficients in projectile	$a_p \stackrel{d}{=} (-)$
Mechanical equivalent of heat	$J \stackrel{d}{=} (-)$

If one needs other specific energies, they can be included in  $a_p$  or  $a_t$  by making ratios with  $E_p$  or  $E_t$ . Phase changes are included with the quantities  $n_p$  and  $n_t$ . The quantities  $C_p$  and  $C_t$  may be superfluous, but will be included for completeness. The reason for inclusion of  $J$  is best stated by the following quote from page 285 of Reference 5.

"Thermal modeling involves at least one more dimension--temperature--than the purely mechanical problems emphasized so far in this book. In Chapter 1 it was brought out that, by considering the statistical mechanics of small particles, the temperature can be expressed in dimensions of energy; however, this forces us to treat one of the constants of statistical mechanics (say Boltzmann's constant or the gas constant) as an abstract number in our list of relevant parameters for every thermal modeling problem. Rather than do this, we follow the customary practice of introducing temperature  $\theta$  as a fourth fundamental dimension. Thus, four dimensions are necessary in thermal modeling, mass  $M$ , length  $L$ , time  $T$ , and temperature  $\theta$ .

"Thermal energy (heat) is usually measured in nonmechanical energy units such as British Thermal Units (BTU) or calories, which appears then as a fifth fundamental dimension. If heat is measured in these thermal units (say BTU's), and mechanical energy is measured in mechanical units (say foot-pounds), we must include the 'mechanical equivalent of heat' in our lists of relevant parameters. Again, rather than introduce another constant, we will measure heat in mechanical units, or convert it to mechanical units, for the purposes of conducting a dimensional analysis. The reader is cautioned, however, that most tabulated values of thermal quantities are given in thermal units so that a conversion of units with the aid of the mechanical equivalent of heat (for example, 1 BTU = 772.28 ft-lb) is needed to make actual calculations. In the system of dimensions used in this book, all quantities that customarily have the units of BTU's or calories will have dimensions of  $FL$  in an  $F, L, T, \theta$  system or  $ML^2T^{-2}$  in an  $M, L, T, \theta$  system."

Note that there are no parameters defining heat conduction processes in either target or projectile. As is true for strain-rate effects, we feel that heat conduction need not be scaled, but for different reasons. The basic reason is that the process of high-velocity penetration is much too rapid for significant conductive heat transfer to occur. Local heating can occur and will probably be very important, but conduction from regions at high temperature to those at low temperature is a relatively slow process, even for good heat conductors like metals. In rapid processes such as this, it is no accident that a predominant failure mechanism is postulated to be adiabatic shear. This implies a process occurring so rapidly that there is no time for heat to transfer away from areas which have been heated by the mechanical work they have undergone.

Generally, in this problem, we are concerned with continuum properties of the projectile materials. Typical interatomic distances in metals are  $3 \times 10^{-7}$  mm, while our smallest caliber model penetrator or thinnest model armor will be about 6 mm. Grain sizes for high-strength metal alloys are, however, about 0.03 mm, which can be of the order of size of some small spall particles. We have already mentioned that a typical flaw size is included in  $K_c$ . To include other microscopic (but not submicroscopic) properties such as grain size and shape in the analysis, we need list only a few more lengths  $l_i$  and angles  $\alpha_i$ .

To complete our list of parameters, we must include ones which describe the results or response in either model or prototype tests. Strains or displacements, either transient or permanent, are already included. We are interested in the time sequence or history of events, so we now add time  $t \stackrel{d}{=} (T)$ . Projectile residual velocity  $V_r \stackrel{d}{=} (L/T)$  and residual mass  $M_r \stackrel{d}{=} (FT^2/L)$  must be recorded. We wish also to characterize back surface spall, but this has already been covered in our discussion of geometric parameters. We add only the total mass of spall fragments  $m \stackrel{d}{=} (FT^2/L)$ .

Our complete list of 48 physical parameters is given in Table 6. Even though we have attempted to reduce the number of parameters by use of shorthand notation, the list is still formidable. Some quantities are redundant, but are included for convenience. As an example, we list wave transmission velocities for projectile and target, even though these parameters are implied by the inclusion of elastic and plastic moduli and densities through the relation

$$c = \left[ \frac{1}{\rho} \left( \frac{\partial \sigma}{\partial \epsilon} \right) \right]^{1/2} \quad (9)$$

The inclusion of redundant parameters will not affect the validity of the model analysis, but will result in more dimensionless pi terms than the minimum necessary. Parameters specifically omitted include strain rates, heat conductivities, and gravity.

#### B. Model Analysis

The next step in a model analysis is to create nondimensional products or pi terms from the list of parameters in Table 6. Many texts exist describing various mathematical procedures for creating pi terms from a list of parameters.<sup>5</sup> Because no new assumptions are involved and the mathematics, unless pi terms are written by inspection (the procedure used herein), are tedious, only the results will be presented. In making this step, no assumptions are introduced into the analysis.

TABLE 6. LIST OF PARAMETERS

Parameter	Symbol	Fundamental Units of Measure
<b>I. Penetrator Properties</b>		
<b>A. Geometric and Impact</b>		
caliber	d	L
other geometric projectile lengths	$l_i$	L
angle of impact	$\beta$	-
yaw angle at impact	$\delta$	-
ogive and other projectile angles	$\alpha_i$	-
velocity of impact	$v_s$	L/T
initial mass	$M_s$	$FT^2/L$
<b>B. Material</b>		
density of projectile	$\rho_p$	$FT^2/L^4$
characteristic projectile stress or strength	$\sigma$	$F/L^2$
other projectile strengths	$\sigma_{ij}$	$F/L^2$
characteristic strain in projectile	$\epsilon_p$	-
other strains	$\epsilon_{pij}$	-
internal energy in projectile	$E_p$	$L^2/T^2$
nondimensional material coefficients in projectile	$a_p, s_p$	-
specific heat of projectile	$C_p$	$L^2/RT^2$
flight temperature of projectile	$\theta_p$	$\theta$
melting temperature of projectile	$\phi_p$	$\theta$
heat of fusion for projectile	$n_p$	$L^2/T^2$
wave transmission velocities	$c_p$	L/T
fracture toughness	$K_{ep}$	$F/L^{3/2}$
<b>II. Target Properties</b>		
<b>A. Geometric</b>		
target thickness for principal armor plate	h	L
thickness of other armor plates	$h_i$	L
space between armor plates	$x_i$	L
<b>B. Material</b>		
density of target material	$\rho_t$	$FT^2/L^4$
characteristic strength of target	S	$F/L^2$
other target strengths or stresses	$S_{ij}$	$F/L^2$
characteristic strain in target	$\epsilon_t$	-
other strains	$\epsilon_{tij}$	-
internal energy in target	$E_t$	$L^2/T^2$
nondimensional material coefficients for target	$a_t, s_t$	-
specific heat of target plates	$C_t$	$L^2/RT^2$
initial temperature of targets	$\theta_t$	$\theta$
melting temperature of target materials	$\phi_t$	$\theta$
heat of fusion for target materials	$n_t$	$L^2/T^2$
wave transmission velocities	$c_t$	L/T
fracture toughness	$K_{ct}$	$F/L^{3/2}$
<b>III. Response Parameters</b>		
time or duration of event	t	T
residual velocity of projectile	$v_r$	L/T
residual mass of projectile	$M_r$	$FT^2/L$
number of spall fragments	N	-
total mass of spall fragments	$m$	$FT^2/L$
velocities of spall fragments	$u_i$	L/T
subsequent reference angles for spall or projectile exit trajectories	$\gamma_i$	-
distribution functions for masses or sizes of spall fragments, velocities of spall fragments, etc.	$f_i$	-
resulting spall or projectile characteristic mean size	r	L
	J	-

Many sets of pi terms are possible. One such set that is complete is given in Table 7. The pi terms in Table 7 are organized into groups for purposes of discussion. Because we have 48 physical parameters, less 4 fundamental dimensions, there are  $48 - 4 = 44$  pi terms.

Similitude theory states that for two systems to be identical, the pi terms in the model and prototype systems must be identical. Note that individual parameters or variables can differ between both systems, provided these differences are achieved while maintaining equality in pi terms. This fact suggests that tests might be run on smaller and less expensive systems than prototype or full-scale ones; however, pi terms must be evaluated to determine if the equality between model and prototype systems can be maintained.

The first nine pi terms state that both model and prototype systems shall be geometrically similar. In other words, all geometric dimensions in the model when divided by the corresponding dimensions in the prototype shall have the same geometric scale factor  $\lambda$ , and all corresponding angles in model and prototype systems shall be identical, i.e., have a scale factor of one. If these two criteria are maintained, geometric similarity is maintained and these nine pi terms are invariant. Pi term 40 is a universal constant and can be dropped because it is invariant in any problem. All pi terms which include single parameters represent quantities which are already dimensionless and must remain so if the scaling law is to be valid.

The remainder of the pi terms can be used to establish relations between scale factors. For example, pi term 11 requires that:

$$\lambda_m = \lambda_{\rho_p} \lambda^3 \quad (10)$$

In words, this equation states that the scale factor for total mass of spall fragments equals the scale factor for projectile density times the cube of the geometric scale factor. The complete set of such relations is given in Eq. (11).

$$\begin{aligned} \lambda_{\rho_t} &= \lambda_{\rho_p} \\ \lambda_m &= \lambda_{M_s} = \lambda_{M_r} = \lambda_{\rho_p} \lambda^3 \\ \lambda_{\theta_p} &= \lambda_{\theta_t} = \lambda_{\phi_t} = \lambda_{\phi_p} \\ \lambda_{V_r} &= \lambda_{V_s} = \lambda_{u_i} = \lambda_{c_p} = \lambda_{c_t} \quad (\text{continued}) \end{aligned}$$

TABLE 7. LIST OF PI TERMS

$\pi_1 = \frac{h}{d}$	} geometric similarity	$\pi_{22} = \frac{C_c}{C_p}$	} similar specific heats	} constitutive similarity
$\pi_2 = \frac{\lambda_i}{d}$		$\pi_{23} = \frac{E_c}{E_p}$		
$\pi_3 = \frac{h_f}{d}$		$\pi_{24} = \frac{\sigma_{ij}}{\sigma}$	} similar stress ratios	
$\pi_4 = \frac{x}{d}$		$\pi_{25} = \frac{S}{\sigma}$		
$\pi_5 = \frac{r}{d}$		$\pi_{26} = \frac{S_{ij}}{\sigma}$		
$\pi_6 = \alpha_1$		$\pi_{27} = \epsilon_p$	} constitutive similarity	
$\pi_7 = \beta$		$\pi_{28} = \epsilon_t$		
$\pi_8 = \gamma$		$\pi_{29} = a_p$		
$\pi_9 = \delta$		$\pi_{30} = a_c$		
$\pi_{10} = \frac{\rho_t}{\rho_p}$	$\pi_{31} = \epsilon_{pij}$			
$\pi_{11} = \frac{m}{\rho_p d^3}$	$\pi_{32} = \epsilon_{tij}$			
$\pi_{12} = \frac{M_s}{\rho_p d^3}$	$\pi_{33} = s_p$			
$\pi_{13} = \frac{M_r}{\rho_p d^3}$	$\pi_{34} = s_t$			
$\pi_{14} = \frac{u_p}{\theta_t}$	$\pi_{35} = K_{cp}/\sigma d^h$			
$\pi_{15} = \frac{\phi_c}{\theta_t}$	$\pi_{36} = K_{ct}/\sigma d^h$			
$\pi_{16} = \frac{\phi_t}{\theta_t}$	$\pi_{37} = N$	} spall similarity		
	$\pi_{38} = f_i$			
$\pi_{17} = \frac{V_r}{V_s}$	$\pi_{39} = \frac{V_s t}{d}$	} kinematic similarity		
$\pi_{18} = \frac{u_i}{V_s}$	$\pi_{40} = J$		} ratio of mechanical energy to thermal energy	
$\pi_{19} = \frac{c_p}{V_s}$	$\pi_{41} = \frac{V_s^2}{E_p}$	} ratio of kinetic energy to material specific energy		
$\pi_{20} = \frac{c_t}{V_s}$	$\pi_{42} = \frac{\rho_p V_s^2}{\sigma}$		} ratio of kinetic energy to strain energy	
$\pi_{21} = \frac{n_t}{n_p}$	$\pi_{43} = \frac{\rho_p n_p}{\sigma}$	} ratio of energy for phase change to strain energy		
	$\pi_{44} = \frac{c_p c_t}{\sigma}$		} ratio of energy to raise material temperature to strain energy	

$$\begin{aligned}
\lambda_{n_t} &= \lambda_{n_p} \\
\lambda_{C_t} &= \lambda_{C_p} \\
\lambda_{E_t} &= \lambda_{E_p} \\
\lambda_{\sigma} &= \lambda_{\sigma_{ij}} = \lambda_s = \lambda_{s_{ij}} \\
\lambda_{K_{c_p}} &= \lambda_{K_{c_t}} = \lambda_{\sigma} \lambda^{1/2} \\
\lambda_{V_s} &= \lambda_t = \lambda \\
\lambda_{V_s}^2 &= \lambda_{E_p} \\
\lambda_{\sigma} &= \lambda_{\rho_p} \lambda_{V_s}^2 = \lambda_{\rho_p} \lambda_{n_p} = \lambda_{\rho_p} \lambda_{C_p} \lambda_{\theta_p}
\end{aligned} \tag{11}$$

Table 7 and the set of equations (11) constitute the results of the similitude analysis. They are too general to be of much use, so we must make further restrictions or assumptions to tell us where this analysis leads us.

### C. Implications of "Replica" Modeling

One choice which automatically satisfies many pi terms is to assume replica modeling. In a replica model, complete geometric similarity is assumed, and all materials in homologous locations in model and prototype are assumed to be identical. Let us turn to Table 7 and follow through the implications of this set of assumptions.

We have already noted that pi terms 1 through 9 are satisfied by maintaining geometric similarity. This is true for a replica model except in the microstructure of the projectile and target materials. By maintaining the same materials, grain sizes are the same rather than scaled by  $\lambda$ .

The next four pi terms, pi 10 through 13, state that similar density ratios should be maintained for both distributed and lumped masses in model and prototype systems. If model and prototype targets as well as penetrators are made of the same material, then these ratios will be the same in both systems provided geometric similarity is also maintained. For a model made of the same material, the densities will be

the same in homologous locations, and the total masses of a model relative to its prototype will scale as the cube of the geometric scale factor  $\lambda^3$ .

Pi terms 14 through 16 state that similar temperatures and melting points must be maintained between model and prototype systems. Once again, if the same initial conditions are maintained and the same material is used in homologous locations, melting points will be identical in model and prototype systems, and these pi terms will be satisfied. These terms imply that if a prototype penetrator undergoes significant heating in launch or flight, a model projectile should also be exposed to this heating, if a model is to be strictly correct.

Pi terms 17 through 20 say that all velocities will be scaled in the same manner.

Similarities for various material properties are covered by pi terms 21 through 36. If the same materials are used at homologous locations in model and prototype, all but two of these terms will be satisfied. Pi term 21 states that heats of fusion must be similar, pi term 11 requires similar specific heats, and pi terms 23 through 36 are statements of constitutive similarity. All but pi terms 35 and 36 are satisfied by the use of identical materials. These terms require that [see Eq. (11)],

$$\lambda_{K_c p} = \lambda_{K_c t} = \lambda_0 \lambda^{1/2} \quad (11a)$$

But,  $\lambda_0 = 1$  for a replica model, so

$$\lambda_{K_c p} = \lambda_{K_c t} = \lambda^{1/2} \quad (11b)$$

Comparing with Eq. (6), we see that the replica modeling requires that the length of critical flaw should scale as  $\lambda^{1/2}$  because the fracture energy  $\Delta_f$  is an intrinsic property of the material, which is unchanged. Our assumption of complete geometric scaling would require that flaws be scaled in the model by factor  $\lambda$ , whereas in reality  $l_f$  will be unchanged between model and prototype, and  $\lambda_{K_c} = 1$ . The dependence of fracture toughness on scale factor in Eq. (11b) is weak, however, because the scale factor is raised to the one-half power.

Pi terms 37 and 38 simply state that the same number of fragments can be expected within the same scaled distributions. Pi term 39 tells

us how to interpret time in a model relative to the prototype. This pi term can be termed a statement of kinematic similarity. If time is interpreted as required,  $\lambda_t = \lambda$  in a replica model, pi term 39 will automatically be satisfied.

The last five pi terms are ratios of energy. They interrelate thermal effects, mechanical ones, inertial effects, energies for phase changes, and specific energies for material states. It is these five terms that determine scale factors for this modeling problem. Similarity pi terms as discussed earlier only state that all lengths, velocities, densities, stresses, temperatures, energies, heats of fusion, and specific heats will be scaled in the same respective fashion. In this problem, all of the pi terms representing energy ratios can be satisfied if the same materials are used in homologous locations in the model as in the prototype. Pi terms 41 and 42 then tell us that we want the same velocities in the model as in the prototype at homologous locations and times.

The assumptions inherent in replica modeling have reduced the relations between scale factors in Eq. (11) to the point that scale factors for all physical parameters in the problem are either fixed, or can be immediately expressed in terms of the geometric scale factor  $\lambda$ . The results are summarized in Table 8.

This particular reduction of the model law in Table 7 is a very powerful one and has already been well validated for projectile impacts in the low velocity and fluid impact regions (see Ref. 5 and Section II). The distortions which occur (parameters which do not exactly scale) are minor and relate entirely to the microstructure of projectiles and target materials. Adherence to replica modeling requires use of identical materials in model and prototype, so lengths such as average grain size and flaw size are unchanged rather than being proportionately smaller in the model.

Effects which we omitted before conducting the model analysis are strain rate effects, gravitational effects, and heat conduction effects. We have given our reasons for omission of rate effects. Because armor is so overstrength relative to dead weight effects, failure to model gravity has no significant influence on spall or breakup. But, "far-field" fragment trajectories are incorrectly scaled. To scale gravitational effects would require a force field in the model that was larger than in the prototype by a factor of  $1/\lambda$ . Although localized heating and material phase changes because of heating are being simulated, heat transfer because of conduction is not being simulated. To model conduc-

tion would add a pi term  $\frac{k\theta d}{\sigma v_s^5}$  to this analysis, and in a replica

model would cause  $k$  to be scaled as  $1/\lambda$ . But  $k$  is a material property; hence, it would be the same in both model and prototype if a replica

TABLE 8. LIST OF SCALE FACTORS FOR  
REPLICA MODEL

<u>Quantities</u>	<u>Symbols</u>	<u>Scale Factors</u>
lengths	$d, h, l, h_i, x, r$	$\lambda$
angles	$\alpha_i, \beta, \lambda, \delta$	1.0
densities	$\rho_p, \rho_t$	1.0
lumped masses	$m, M_s, M_r$	$\lambda^3$
temperatures	$\theta_p, \theta_t, \phi_p, \phi_t$	1.0
velocities	$V_r, u_i, v_s, c_p, c_t$	1.0
heats of fusion	$n_t, n_p$	1.0
specific heats	$C_t, C_p$	1.0
internal energies	$E_t, E_p$	1.0
stresses	$\sigma_{ij}, \sigma, S, S_{ij}$	1.0
strains	$\epsilon_p, \epsilon_t, \epsilon_{pij}, \epsilon_{tij}$	1.0
nondimensional material coefficients	$a_p, a_t, s_p, s_t$	1.0
number of fragments	$N$	1.0
time	$t$	$\lambda$
mechanical equivalent of heat	$J$	1.0
fracture toughnesses	$K_{cp}, K_{ct}$	$\lambda^{\frac{1}{2}}$
distribution functions for spall fragments	$f_i$	1.0

modeling law is applied. Failure to scale  $k$  appropriately means that heat is not carried away fast enough in the model system. Probably this error is insignificant, as durations are so short in both model and prototype systems that no energy can be dissipated through this transfer mechanism.

We feel that these distortions should have little effect on scaling of the penetration process, wave transmission effects, and even gross plastic deformations and phase changes. What may be affected is the exact character of back surface spall or projectile breakup because

these processes are probably a function of the material microstructure and sizes of flaws. Experimental tests are required so comparisons can be made to assess the importance of material microstructure on spall and breakup.

#### D. Implications of Dissimilar Material Modeling

The general model law in Table 7 can perhaps be reduced to a practical law by at least one other set of assumptions than those inherent in replica modeling. This set of assumptions is termed "dissimilar material modeling" in Reference 5 and is discussed in some detail in Chapter 7 of that reference. In a dissimilar material model, the model materials are related to those in the prototype by requiring that they have constitutive similarity, or have similar dimensionless stress-strain curves, at appropriate strain rates. This concept is shown schematically in Figure 10. For exact constitutive similarity, the entire scaled curves should match, up to ultimate stress and strain. But, for scaling involving large plastic deformations, good correlations can be achieved if one merely requires equivalence of the integrals of the scaled stress-strain curves, or areas under these curves. The materials can be dissimilar in densities, microstructure, and other properties as long as they exhibit constitutive similarity.

If we assume geometric similarity and constitutive similarity in the sense just discussed, then the feasibility of applications of dissimilar material modeling to high velocity penetration hinges on finding whether there exist model materials, different from the prototype materials, which satisfy the other significant scaling relationships in Table 7 or Eq. (11). There are some approximate physical relationships which can help in this search.

First, many high strength metals have nearly the same sound velocities, defined by

$$c_o = (E/\rho)^{1/2} \approx 5000 \text{ m/s} \quad (12)$$

Constitutive similarity then requires, through the relation (9), that all waves at scaled stress levels will propagate at about the same velocities. In our model analysis, this translates to the requirement

$$\lambda_{c_o} = \lambda_{c_p} = \lambda_{c_t} = 1 \quad (13)$$

Second, the heats of fusion  $h$  can be shown to be proportional to the square of the sound velocity for most metals (see p. 192 of Ref. 5), i.e.,

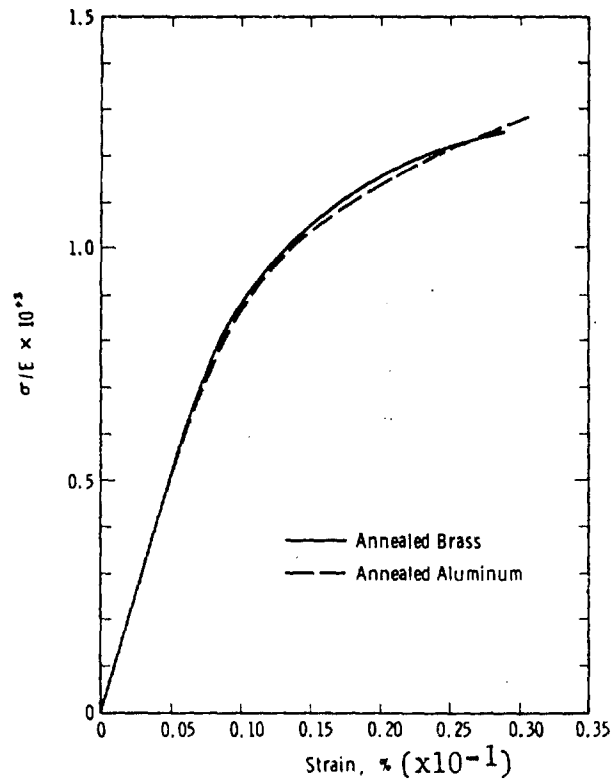


FIGURE 10. STRESS-STRAIN CURVES FOR MATERIALS POSSESSING CONSTITUTIVE SIMILARITY(5)

$$c_o^2 = (E/\rho) = C_1 n \quad (14)$$

where  $C_1$  is a constant which is independent of the metal. But, we have just said that  $c_o$  is an invariant. So, Eqs. (14) and (13) require that heats of fusion be invariant for high strength metals

$$\lambda_{n_p} = \lambda_{n_t} = 1 \quad (15)$$

Third, it is shown on p. 191 of Reference 5 that the melting temperature of metals  $\phi$ , the specific heat  $C$ , and the heat of fusion are related so that

$$\frac{\phi C}{n} = C_2 \quad (16)$$

where  $C_2$  is a constant. This then tells us that

$$\lambda_\phi = \frac{1}{\lambda_C} \quad (17)$$

for either target or projectile material.

By inserting the restrictions of Eqs. (13), (15), and (16) into the relations in Eq. (11), we can construct Table 9 for scale factors in dissimilar material modeling of the penetration process.

TABLE 9. LIST OF SCALE FACTORS FOR DISSIMILAR MATERIAL MODELING

<u>Quantities</u>	<u>Symbols</u>	<u>Scale Factors</u>
lengths	$d, h, l_i, h_i, x, r$	$\lambda$
angles	$\alpha_i, \beta, \gamma, \delta$	1.0
densities	$\rho_p, \rho_t$	$\lambda_\rho$
lumped masses	$m, M_s, M_r$	$\lambda^3 \lambda_\rho$
temperatures	$\theta_p, \theta_t, \phi_p, \phi_t$	$\lambda_\theta$
velocities	$V_r, u_i, V_s, c_p, c_t$	1.0
heats of fusion	$n_t, n_p$	1.0
specific heats	$C_t, C_p$	$1/\lambda_\theta$
internal energies	$E_t, E_p$	1.0
stresses	$\sigma, \sigma_{ij}, s, s_{ij}$	$\lambda_\rho$
strains	$\epsilon_p, \epsilon_t, \epsilon_{pij}, \epsilon_{tij}$	1.0
nondimensional material coefficients	$a_p, a_t, s_p, s_t$	1.0
number of fragments	$N$	1.0
time	$t$	$\lambda$
mechanical equivalent of heat	$J$	1.0
fracture toughness	$K_{cp}, K_{ct}$	$\lambda_\rho \lambda^{1/2}$
distribution functions for spall fragments	$f_i$	1.0

In Table 9, we see that three scale factors now appear,  $\lambda$ ,  $\lambda_\rho$ , and  $\lambda_\theta$ , in contrast to only the geometric scale factor in Table 8. Let us discuss some practical ranges for these factors. We have already said that

$$0.1 \leq \lambda \leq 1 \quad (18)$$

Densities of prototype materials are very high, and we will probably wish the models to be less dense. Assuming that the penetrator is tungsten and the lightest metal we are apt to use in the model is magnesium,

$$0.09 \leq \lambda_\rho \leq 1 \quad (19)$$

Critical temperatures are melting temperatures,  $\phi_p$  and  $\phi_t$ . For the metals we wish to use, these range from 651 C for magnesium to 3370 C for tungsten. So,

$$0.19 \leq \lambda_\theta \leq 1 \quad (20)$$

To aid in choice of materials, a brief table of properties of some metals we might use is included in Table 10. A few alloys are included in the table--many have properties intermediate between those of the elements in the table, except that sound velocities are often higher for the alloys.

Without more exhaustive study, it appears feasible to use lighter metals for model tests than for prototype tests. If the prototype situation were a tungsten alloy penetrator impacting spaced steel armor, a possible model combination would be a brass or steel penetrator impacting titanium alloy targets, or a titanium penetrator impacting an aluminum alloy or magnesium alloy target. Although Table 9 shows that impact velocities would be identical to prototype velocities, cheaper or more readily available materials could be used, and the lower densities would mean lighter projectiles which could be more easily launched at high velocity. Proportionately lower yield and ultimate stresses in the materials would ease machining problems. Scaling of melting temperatures and specific heats is accomplished [see Eqs. (16) and (17)], wave transmission effects scale, inertial effects scale, and times scale by the geometric scale factor  $\lambda$  as for replica modeling. Scaling of fracture toughness per se is not accomplished, but perhaps one can come close by adjusting grain size or flaw size in the model. It has already been well documented<sup>5</sup> that dissimilar material modeling is possible in the fluid impact region, but of course many fewer parameters are important in this region.

TABLE 10. SOME PROPERTIES OF METALS

<u>Metal</u>	<u>Density</u> $\rho$ (Mg/m <sup>3</sup> )	<u>Specific</u> <u>Heat</u> $c$ (cal/g°C)	<u>Melting</u> <u>Temperature</u> $\phi$ (C)	<u>Sound</u> <u>Velocity</u> $c_o$ (m/s)
Magnesium	1.74	0.243	651	5050
Aluminum	2.76	0.215	660	5000
High Strength Steel	7.85	0.017	1500	5100
Iron	7.85	0.017	1535	3800
304 Stainless Steel	7.90	0.037	1430	4570
Titanium	4.51	0.0540	1675	5100
Naval Brass	8.41	0.090	900	3750
Uranium	18.45	0.0278	1132	2570
Molybdenum	10.22	0.060	2610	5120
Tungsten	19.30	0.034	3370	4220
Tungsten Carbide	(10-15.6)	≈0.03	(2500-2800)	4920
Copper	8.93	0.092	1083	3940

#### IV. DISCUSSION

A rather general similitude analysis is presented in Section III, together with the implications of this analysis for replica and dissimilar material modeling assumptions. Because a very large number of material parameters were included in the analysis, it is not possible to simultaneously satisfy (keep invariant) all of the dimensionless parameters for sub-scale testing with either a replica or dissimilar material model. But, the vast majority of the pi terms do remain invariant for either set of assumptions, and sub-scale testing appears feasible.

The possible advantages of a replica model are:

- (1) Exact matching of scaling requirements for most material constitutive properties in both penetrator and target materials,
- (2) Exact matching of thermal properties and phase change properties,
- (3) A body of existing data for simpler penetrators versus monolithic armor that demonstrates validity of the replica modeling law.

Disadvantages of a replica model are:

- (1) Microstructure of the materials and effects such as back-surface spall, which are probably affected, do not scale.
- (2) Fracture toughness does not strictly scale, although the dependence on scale factor is small.
- (3) Even on a model scale, costs of making penetrators of exotic materials may be very expensive and time-consuming.

The possible advantages of a dissimilar material model are:

- (1) Both penetrator and target can be made of relatively cheap and available materials.
- (2) Because the model materials will in general be lighter and of lower strength than prototype materials, models should be much less expensive to make and more easily launched.
- (3) It may be possible, by proper choice of model materials, to scale microstructure and fracture toughness.

Disadvantages of a dissimilar material model are:

- (1) Constitutive properties are modeled approximately, but not exactly, so scaling is less exact.
- (2) The concept of dissimilar material modeling may be more difficult to "sell" to the uninitiated.

In the general model law (and hence, in either the replica or dissimilar material laws), several physical processes which do not scale are deliberately omitted. We feel that there is ample experimental evidence for these omissions, and present that evidence in earlier sections. Gravity effects are omitted as unimportant in high velocity impacts; strain-rate effects on constitutive properties do not differ enough between model and prototype to significantly affect scaling; and the penetration process is too rapid for significant conductive heat transfer to occur.

The similitude analysis includes more geometric parameters than does the earlier one of Reference 5 and Table 2 because geometry of both the projectile and the spaced armor target are more complex. But, the scaling of more lengths and angles does not change the basic model law one iota! One still has the requirement of absolute geometric similarity between model and prototype. The inclusion of more geometric parameters to completely define thicknesses and spacings in the spaced armor does require much more testing and/or calculation to evaluate the effect of varying these dimensions on penetrators. Then, too, the second and later layers in the spaced armor can be impacted by a cloud of armor spall particles and a deformed or shattered penetrator. Constitutive properties for all materials are properly scaled through large deformations and may affect the number and size of spall particles. Possibly, penetration through the first layer of spaced armor will be accurately modeled, while penetration through later layers will not.

What is the smallest practical scale for model testing? Conceptually, the lower limit on geometric scale is fixed by the necessity to have the smallest linear dimension of either projectile or armor layers significantly larger than mean grain size. We have said earlier that average grain size for high yield alloys is about 0.03 mm, so we probably want the minimum model dimension to be about ten times this value, or 0.3 mm. The necessity to maintain closer manufacturing tolerances on the model than on the prototype (these scale by  $\lambda$  like any other lengths) introduces a more practical lower limit to size. An existing long-rod penetrator has a caliber  $d = 20.65 \pm 0.25$  mm. A model with a reasonably small scale factor of  $\lambda = 0.1$  would have a caliber of  $d = 2.065 \pm 0.025$  mm. This increase in tolerance is possible to maintain, but another order of magnitude decrease would be practically impossible, or at least very expensive.

The model scale is probably best chosen to match existing gun systems capable of launching rounds with discarding sabots. Returning to Figure 4, we see a projectile which in full scale is designed for launching from a barrel with a 75-mm bore. The projectile itself has a largest lateral dimension  $\ell_3 = 54.0$  mm, a caliber  $d = 20.65$  mm, and a length  $\ell_4 = 305$  mm. A popular launch tube for precision range testing is a 20-mm bore barrel. Using this cannon, we would suggest a scale factor  $\lambda = 20 \text{ mm}/75 \text{ mm} = 0.267$ . Then, a model projectile could be launched using geometrically similar sabots and dimensions  $\ell_3 = 54.0 \times 0.267 = 14.4$  mm,  $d = 20.65 \times 0.267 = 5.51$  mm, and  $\ell_4 = 305 \text{ mm} \times 0.267 = 81.4$  mm. The minimum dimension for this projectile is the thickness of the aluminum fin material, 1.52 mm. In the model this thickness is  $1.52 \times 0.267 = 0.407$  mm, which approaches the lower limit of ten times grain size. A still smaller caliber model of this particular projectile might prove difficult to hold within manufacturing tolerances, or have fins which are below our somewhat arbitrary grain size limit.

How will one know that either the replica or dissimilar material model laws suggested here are correct? This question cannot be answered until comparisons can be made between tests conducted on different geometric scales and/or with different materials. Even then, the answers can be at best probabilities that the model data correlate with the prototype data, with some level of confidence.

Measured parameters which can conceivably be compared between model and prototype are:

- (1) Velocities  $V_s$ ,  $V_r$ ,  $u_i$ ,
- (2) Dimensions and shapes of holes in armor,  $\ell_i$ ,  $\alpha_i$ ,
- (3) Characteristics of spall  $N$ ,  $f_i$ .

Test data for velocities  $V_s$  and  $V_r$  are usually presented graphically as in Figure 11 and fitted to empirical equations such as the one inset in the figure. For residual velocity data for model-prototype comparison, curves or data such as those in Figure 11 would first be rendered non-dimensional by using appropriate pi terms and then would be analyzed statistically.

Various methods of statistical comparison of scaled model and prototype data are possible. Scaled data for residual velocity versus impact velocity consist essentially of plots or tables of  $\pi_{17}$  as a dependent variable versus  $\pi_{42}$  (or its square root) as the independent variable, all other pi terms being held constant. If model tests are

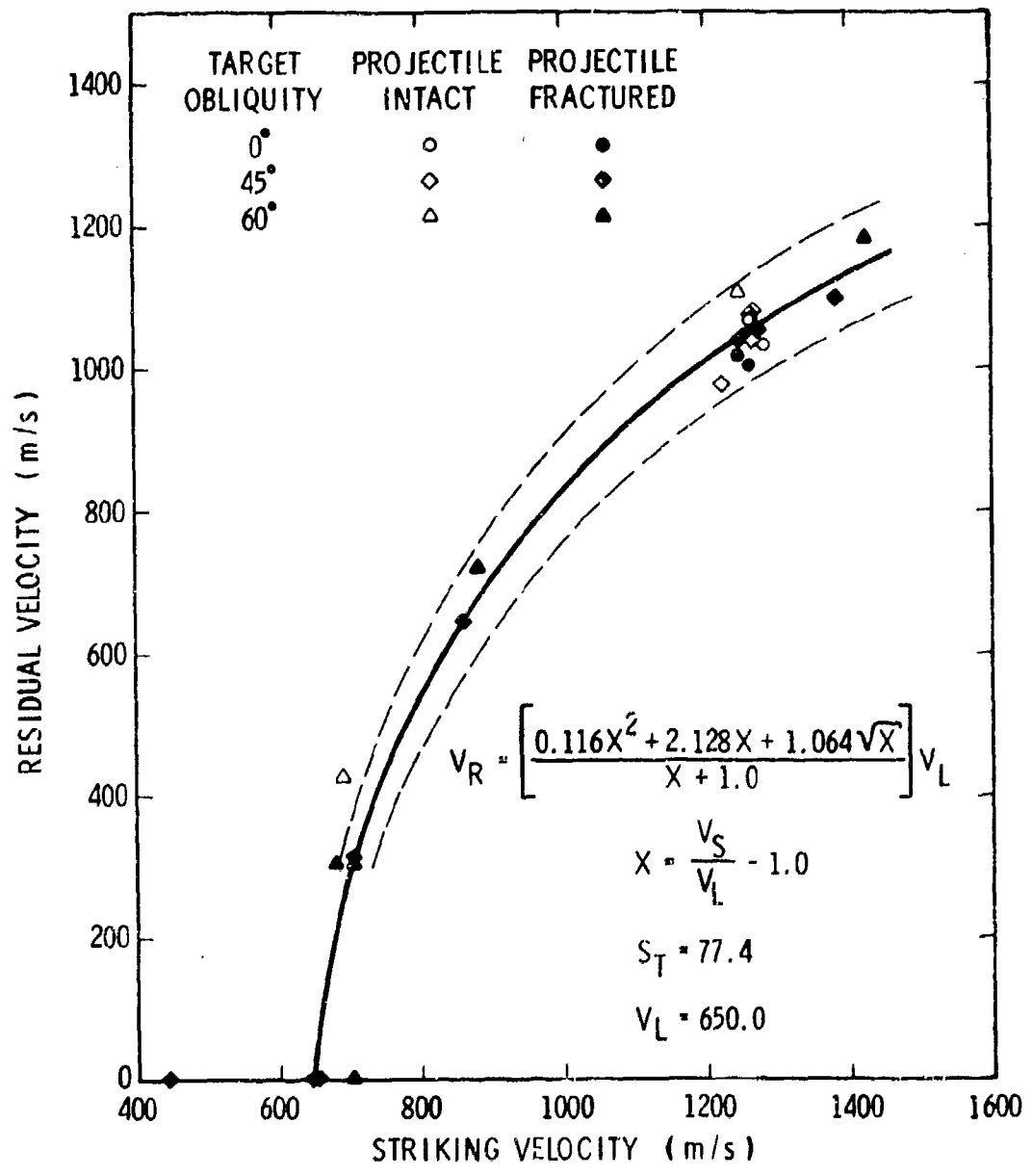


FIGURE 11. COMPARISON OF SINGLE AND TRIPLE TARGET TESTS<sup>(8)</sup>

designed to reproduce, as closely as possible, prototype values of the independent variable, then perfectly standard statistical tests can be made to compare the values of the scaled dependent variables for identical values of scaled independent variable. The standard statistical tests one would use are Students "T" test to compare means of the data, and the F test to compare variances (standard deviations). If, on the other hand, values of the scaled independent variable do not match, the simple T and F tests are inapplicable. In this instance, one can still use standard statistical methods for comparing multiple regression coefficients. following fitting of scaled prototype and model data to some empirical equation, as in Figure 11. Reference 13 is a good source for the standard statistical methods we have mentioned.

An alternative method for comparing scaled model and prototype data is given on pp. 352-356 of Reference 5. This procedure involves fitting model and prototype data individually to some appropriate empirical equation. normalizing each set of data, and computing a standard deviation about each normalized curve. Then, one uses Students "T" test to compute three probabilities, i.e.,

- (1) Measured model results being within a specific tolerance of other model results,
- (2) Measured prototype results being within the same tolerance for other prototype results,
- (3) Scaled prototype and model results being within the same tolerance for other scaled results.

Finally, one computes a "degree of association" of model and prototype scaled data. This percentage is the probability that all data (both model and prototype) correlate, divided by the poorer of the probabilities (1) and (2). A high percentage value for this last quantity indicates good agreement between model and prototype data.

To compare hole sizes in armor, various dimensions of the holes would be measured and scaled profiles compared. Hole volume, or suitable lateral dimensions could then be plotted versus scaled impact velocity, and statistical tests performed in much the same manner as for residual velocity.

The number of spall fragments produced is postulated to be invariant with scale of test, for the same scaled impact velocities, as is some (as yet unknown) set of distribution functions for mass and mean size. These, too, should be determined experimentally as a function of scaled impact velocity for model and for prototype. The distribution functions may be Gaussian or some other function. Their form will determine the specific statistical treatment which will be needed to compare model and prototype data and complete the assessment of the model law or laws.

For both model and prototype tests, enough replications of a given test must be run to obtain reasonable confidence limits in the test data. By fitting to empirical functions, exact replication is not required, and is indeed quite difficult. For a given projectile-armor-obliquity combination, it seems from past experience<sup>8</sup> that 8 to 15 model or prototype tests over a range of impact velocities may be sufficient to acquire the test data for validation of a model law. Only after reviewing existing prototype data can one determine the needed number of model tests more exactly.

## V. RECOMMENDATIONS

Two possible specific model laws evolved in our model analysis. Both require complete geometric similarity and identity of all velocities. In the first, termed the "replica law," all penetrator and armor materials are identical in homologous locations in model and prototype. In the second, termed the "dissimilar material law," model and prototype materials must have constitutive similarity, but the model projectile and targets can both be made of lighter and weaker materials than in the prototype. Both laws must rely on what we feel are minor distortions for their validity, and both have their advantages and disadvantages.

For reasons discussed above, we recommend two sets of model scale experiments designed to model existing test data for long rods penetrating spaced armor. Hopefully, there are sufficient full-scale data available to define the response parameters which should be measured in each test (see Section IV). If this is not the case, additional full-scale tests may have to be conducted, with careful attention to measurement of velocities, hole sizes and dimensions, masses and sizes of ejecta, etc. We recommend both replica model tests and dissimilar material model tests, with 8 to 15 tests of each type with a single design of penetrator and spaced target at a single impact obliquity.

If we are modeling the projectile discussed earlier, a good candidate for geometric model scale is  $\lambda = 0.267$ , and a good candidate for a launching gun is a 20-mm smooth bore. A brass penetrator and titanium alloy target material may be an acceptable combination to model U-(3/4) Ti penetrators versus rolled homogeneous steel armor. Titanium alloy sheet is readily available in many gages, and brass is a cheap, easily machined material for a penetrator. All tests should be well instrumented with velocity screens, flash x-ray equipment, and spall retrieval systems.

A number of supporting test and material data should be obtained. Complete dynamic material properties should be measured, preferably at strain rates  $\geq 10^3/s$ . Each projectile should be accurately weighed and x-rayed to detect flaws. Fracture toughness data should be reviewed, and additional data obtained if too little are available. Average grain size and shape of virgin projectile and target material should be obtained by metallographic examination. Post-test metallographic examination of recovered projectile pieces and perforated targets may prove desirable to detect regions of phase changes or adiabatic shear.

We recommend comparison of model and prototype test data on a statistical basis, using methods discussed earlier. Comparisons should be made on the dimensionless response parameters corresponding to residual

velocity  $V_r$ , spall velocities  $u_i$ , dimensions and shapes of holes in armor layers, and numbers  $N$  and distribution functions  $f_i$  of spall fragments. All of these parameters will be functions of scaled impact velocity and the particular combination of penetrator, spaced armor, and impact obliquity.

We believe that careful planning and execution of the model test will indeed validate both the replica and dissimilar material laws for this complex problem. The terminal ballisticians should then be able to invoke some of the savings in money and time which are inherent in most sub-scale testing to evaluate new concepts for high velocity kinetic energy penetrators, or alternatively, to evaluate spaced armor concepts to defeat such penetrators.

#### REFERENCES

1. S. Z. Burstein, H. S. Schechter, and E. Turkel, "An Accurate Numerical Model for Dynamic Problems in Continuum Mechanics," Proc. of the First Int. Symp. on Ballistics, ADPA, Orlando, Fla., Nov. 1974, pp. IV-27 to IV-44.
2. R. T. Sedgwick and L. J. Walsh, "Numerical Techniques for Modeling Armor Penetration and Behind-the-armor Debris," Proc. of the First Int. Symp. on Ballistics, ADPA, Orlando, Fla., Nov. 1974, pp. IV-45 to IV-64.
3. C. W. Curtis, "Terminal Ballistics of Armor," in Summary Tech. Rep. of Div. 2, NDRC, Vol. 1, Effects of Impact and Explosion, Washington, D. C., 1946, pp. 160-190 (AD 221-586).
4. B. R. Killian, "An Empirical Analysis of the Perforation of Rolled and Cast Homogeneous Armor by Conventionally Shaped Kinetic Energy Projectiles of Calibers 37 mm Thru 155 mm," BRL Memorandum Report No. 1083, June 1957. (AD #145533)
5. W. E. Baker, P. S. Westine, and F. T. Dodge, Similarity Methods in Engineering Dynamics, Hayden Book Co., Inc., Rochelle Park, N. J., 1973.
6. J. L. Summers and A. C. Charters, "High-speed Impact of Metal Projectiles in Targets of Various Materials," Proc. of Third Symp. on Hypervelocity Impact, 1, pp. 101-110, Feb. 1959.
7. J. K. Dienes and J. M. Walsh, "Theory of Impact: Some General Principles and the Method of Eulerian Codes," Chapter III in High-velocity Impact Phenomena, R. Kinslow (ed.), Academic Press, New York and London, 1970, pp. 75-104.
8. A. B. Wenzel and J. C. Hokanson, "Effects of Single vs Multiple Targets on Rod Penetration," BRL Contractor Report (in review).
9. N. J. Huffington, Jr. (ed.), Behavior of Materials Under Dynamic Loading, Am. Soc. of Mech. Eng., 1965.
10. U. S. Lindholm and R. L. Bessey, "A Survey of Rate Dependent Strength Properties of Metals," AFML-TR-69-119, April 1969.
11. R. G. McQueen, S. P. Marsh, J. W. Taylor, J. N. Fritz, and W. J. Carter, "The Equation of State of Solids from Shock Wave Studies," Chapter VII in High-velocity Impact Phenomena, R. Kinslow (ed.), Academic Press, New York and London, 1970, pp. 293-417.

12. C. H. Johansson and P. A. Persson, Detonics of High Explosives, Academic Press, London and New York, 1970.
13. G. J. Hahn and S. S. Shapiro, Statistical Models in Engineering, John Wiley & Sons, Inc., New York, 1967.

DISTRIBUTION LIST

<u>No. of Copies</u>	<u>Organization</u>	<u>No. of Copies</u>	<u>Organization</u>
12	Commander Defense Documentation Center ATTN: DDC-TCA Cameron Station Alexandria, VA 22314	2	Commander US Army Missile Command ATTN: DRSMI-R DRSMI-RBL Redstone Arsenal, AL 35809
1	Director Defense Nuclear Agency ATTN: MAJ Spangler Arlington, VA 22209	1	Commander US Army Tank Automotive Development Command ATTN: DRDTA-RWL Warren, MI 48090
1	Director Defense Advanced Research Projects Agency ATTN: Tech Info 1400 Wilson Boulevard Arlington, VA 22209	4	Commander US Army Mobility Equipment Research & Development Command ATTN: Dr. J. Bond Mr. D. Dinger Tech Docu Cen, Bldg. 315 DRSME-RZT Fort Belvoir, VA 22060
1	Commander US Army Materiel Development and Readiness Command ATTN: DRCDMA-ST 5001 Eisenhower Avenue Alexandria, VA 22333	1	Commander US Army Armament Command ATTN: DRSAR-RDT, T. Hung Rock Island, IL 61202
1	Commander US Army Aviation Systems Command ATTN: DRSAV-E 12th and Spruce Streets St. Louis, MO 63166	2	Commander US Army Picatinny Arsenal ATTN: SARPA-AD-EP Mr. V. Guadagno SARPA-AD-D-A-2 Mr. R. Davitt Dover, NJ 07801
1	Director US Army Air Mobility Research and Development Laboratory Ames Research Center Moffett Field, CA 94035	1	Commander US Army Rock Island Arsenal ATTN: SARRI-LA-AC, W. Wells Rock Island, IL 61202
2	Commander US Army Electronics Command ATTN: DRSEL-RD DRSEL-HL-CT Mr. S. Crossman Fort Monmouth, NJ 07703	2	Commander US Army Frankford Arsenal ATTN: SARFA-FCA-W Mr. D. Swartz SARFA-MDA-A Mr. D. Donnelly Philadelphia, PA 19137

DISTRIBUTION LIST

<u>No. of Copies</u>	<u>Organization</u>	<u>No. of Copies</u>	<u>Organization</u>
1	Commander US Army Watervliet Arsenal ATTN: SARWV-RDD-SE, P.Vottis Watervliet, NY 12189	1	Commander US Army Research Office ATTN: Dr. E. Saibel P. O. Box 12211 Research Triangle Park NC 27709
1	Commander US Army Harry Diamond Labs ATTN: DRXDO-TI 2800 Powder Mill Road Adelphi, MD 20783	1	Chief of Naval Research ATTN: Code ONR 439 N. Perrone Washington, DC 20360
5	Commander US Army Materials and Mechanics Research Center ATTN: DRXMR-T, J. Bluhm DRXMR-T, D. Roylance DRXMR-T, A. F. Wilde DRXMR-T, J. Mescall DRXMR-ATL Watertown, MA 02172	3	Commander US Naval Air Systems Command ATTN: AIR-604 Washington, DC 20360
1	Commander US Army Natick Research and Development Center ATTN: BRXPE, Dr. L. Sieling Natick, MA 01761	3	Commander US Naval Ordnance Systems Command ATTN: ORD-9132 Washington, DC 20360
1	Director US Army TRADOC Systems Analysis Activity ATTN: ATAA-SA White Sands Missile Range NM 88002	1	Commander US Naval Air Development Center, Johnsville Warminster, PA 18974
1	Deputy Assistant Secretary of the Army (R&D) Department of the Army Washington, DC 20310	1	Commander US Naval Missile Center Point Mugu, CA 93041
1	HQDA (DAMA-AR) Washington, DC 20310	1	Commander and Director David W. Taylor Naval Ship Research & Development Center Bethesda, MD 20084
1	HQDA (DAMA-MS) Washington, DC 20310	2	Commander US Naval Surface Weapons Center Silver Spring, MD 20910

DISTRIBUTION LIST

<u>No. of Copies</u>	<u>Organization</u>	<u>No. of Copies</u>	<u>Organization</u>
3	Commander US Naval Surface Weapons Center ATTN: Code TEB D. W. Colbertson Mr. L. Hock Code TX, W. G. Soper Dahlgren, VA 22448	1	Headquarters National Aeronautics and Space Administration Washington, DC 20546
3	Commander US Naval Weapons Center ATTN: Code 4057 Code 5114, E. Lundstrom Code 6031, Mr. M. Backman China Lake, CA 93555	1	Director Jet Propulsion Laboratory ATTN: Lib (TDS) 4800 Oak Grove Drive Pasadena, CA 91103
4	Commander US Naval Research Laboratory ATTN: Mr. W. J. Ferguson Mr. J. Baker Dr. H. Pusey Dr. F. Rosenthal Washington, DC 20375	1	Director National Aeronautics and Space Administration Langley Research Center Langley Station Hampton, VA 23365
1	Superintendent US Naval Postgraduate School ATTN: Dir of Lib Monterey, CA 93940	1	Director National Aeronautics and Space Administration Manned Spacecraft Center ATTN: Lib Houston, TX 77058
1	ADTC/DLJW, CPT D. Matyska Eglin AFB, FL 32542	1	Aerospace Corporation ATTN: Dr. L. Rubin P. O. Box 95085 Los Angeles, CA 90045
1	AFATL (DLDL, MAJ J.E. Morgan) Eglin AFB, FL 32542	1	Boeing Aerospace Company ATTN: Mr. R.G. Blaisdell (M.S. 40-25) Seattle, WA 98124
2	AFWL (WLL) Kirtland AFB, NM 87117	1	Computer Code Consultants ATTN: Mr. W. Johnson 527 Glencrest Drive Solana Beach, CA 72025
1	AFEDL (PDT) Wright-Patterson AFB, OH 45433	2	Dupont Experimental Labs ATTN: Mr. J. Lupton Dr. C. Zweben Wilmington, DE 19801
3	ASD (YH/EX; John Rievley; XKHD, Gerald Bennett; ENYS, Matt Kolleck) Wright-Patterson AFB, OH 45433		

## DISTRIBUTION LIST

<u>No. of Copies</u>	<u>Organization</u>	<u>No. of Copies</u>	<u>Organization</u>
1	Falcon R&D ATTN: Mr. R. Miller 1225 S. Huron Street Denver, CO 80223	3	Sandia Laboratories ATTN: Dr. W. Herrmann Dr. L. Bertholf Dr. J. W. Nunziato P. O. Box 5800 Albuquerque, NM 87115
2	Falcon R&D, Thor Facility ATTN: Mr. D. Malick Mr. J. Wilson 696 Fairmount Avenue Baltimore, MD 21204	2	Systems, Science & Software ATTN: Dr. R. Sedgwick Ms. L. Hageman P. O. Box 1620 La Jolla, CA 92038
1	President General Research Corporation ATTN: Lib McLean, VA 22101	3	Brown University Division of Engineering ATTN: Prof. P. Marcal Prof. H. Kolsky Prof. P. Symonds Providence, RI 02192
3	Honeywell, Inc. Government and Aerospace Products Division ATTN: Mr. J. Blackburn Dr. G. Johnson Mr. R. Simpson 600 Second Street, NE Hopkins, NM 55343	2	California Institute of Tech Division of Engineering and Applied Science ATTN: Dr. J. Miklowitz Dr. E. Sternberg Pasadena, CA 91102
1	Lockheed Corporation ATTN: Dr. C. E. Vivian Department 8114 Sunnyvale, CA 94087	2	Carnegie Mellon University Department of Mathematics ATTN: Dr. D. Owen Dr. M. E. Gurtin Pittsburgh, PA 15213
1	McDonnell Douglas Aeronautics Company ATTN: Mail Station 21-2 Dr. J. Wall 5301 Bolsa Avenue Huntington Beach, CA 92647	1	Catholic University of America Schooling of Engineering and Architecture ATTN: Prof. A. Durelli Washington, DC 20017
1	Rockwell Corporation ATTN: Mr. W. Jackson 10301 Overhill Drive Santa Ana, CA 92705	4	Cornell University Dept of Theoretical Applied Mech ATTN: Dean E. Cranch Prof G. Ludford Prof D. Robinson Prof Y-H Pai Ithaca, NY 14850

DISTRIBUTION LIST

<u>No. of Copies</u>	<u>Organization</u>	<u>No. of Copies</u>	<u>Organization</u>
2	Drexel University Dept of Mech Engineering ATTN: Dr. P. C. Chou Dr. F. K. Tsou 32nd and Chestnut Streets Philadelphia, PA 19104	2	Forrestal Research Center Aeronautical Eng Laboratory Princeton University ATTN: Dr. S. Lam Dr. A. Eringen Princeton, NJ 08540
2	Iowa State University Engineering Research Lab ATTN: Dr. G. Nariboli Dr. A. Sedov Ames, IA 50010	1	Purdue University Inst for Mathematical Sciences ATTN: Dr. E. Cumberbatch Lafayette, IN 47907
3	Lehigh University Center for the Application of Mathematics ATTN: Dr. E. Varley Dr. R. Rivlin Dr. A. Kalnins Bethlehem, PA 18015	2	Purdue University School of Aeronautics Astronautics and Engineering Sciences ATTN: Prof. S. Koh Prof. C. Sun Lafayette, IN 47907
2	Massachusetts Inst of Tech ATTN: Dr. R. Probstein Dr. J. Dugundji 77 Massachusetts Avenue Cambridge, MA 02139	2	Rice University ATTN: Dr. Bowen Dr. A. Miele P. O. Box 1892 Houston, TX 87001
1	New York University Courant Institute ATTN: Dr. S. Z. Burstein 251 Mercer Street New York, NY 10012	5	Southwest Research Institute ATTN: Dr. H. Abramson Mr. A. Wenzel Dr. P. Westine Dr. W. Baker Mr. J. Hokanson 8500 Culebra Road San Antonio, TX 78228
1	North Carolina State Univ Dept of Eng Mechanics ATTN: Dr. W. Bingham P. O. Box 5071 Raleigh, NC 27607	1	Stanford Research Institute Poulter Laboratory 333 Ravenswood Avenue Menlo Park, CA 94025
2	Pennsylvania State University Engineering Mechanical Dept ATTN: Prof. Haythornthwaite Prof. N. Davids University Park, PA 16802	1	Stanford University ATTN: Dr. E. H. Lee Stanford, CA 94035

DISTRIBUTION LIST

<u>No. of</u> <u>Copies</u>	<u>Organization</u>	<u>No. of</u> <u>Copies</u>	<u>Organization</u>
1	Swarthmore College Dept of Mathematics ATTN: Prof. D. Rosen Swarthmore, PA 19081	3	University of Delaware Dept of Mechanical Engineering ATTN: Prof. J. Vinson Prof. J. Nowinski Dr. B. Pipes Newark, DE 19711
1	Tulane University Dept of Mechanical Engineering ATTN: Dr. S. Cowin New Orleans, LA 70112	2	University of Denver Denver Research Institute ATTN: Mr. R. F. Recht Mr. T. W. Ipson 2396 South University Blvd Denver, CO 80210
3	University of Arizona Civil Engineering Dept ATTN: Dr. D. A. DaDeppo Dr. R. Richard Dr. R. C. Neff Tucson, AZ 85721	3	University of Florida Department of Engineering Science and Mechanics ATTN: Dr. C. A. Sciammarella Dr. L. Malvern Dr. N. Cristescu Gainesville, FL 32601
2	University of California ATTN: Dr. M. Carroll Dr. P. Naghdi Berkeley, CA 94704	1	University of Houston Dept of Mechanical Eng ATTN: Dr. R. Nachlinger Houston, TX 77004
1	University of California Dept of Aerospace and Mechanical Eng Sciences ATTN: Dr. Y. C. Fung P. O. Box 109 La Jolla, CA 92037	1	University of Illinois at Chicago Circle College of Engineering Dept of Materials Engineering ATTN: Prof. A. Schultz P. O. Box 4348 Chicago, IL 60680
2	University of California Department of Mechanics ATTN: Dr. Stern Dr. S. B. Dong 504 Hilgard Avenue Los Angeles, CA 90024	1	University of Illinois Dept of Theoretical & Applied Mechanics ATTN: Dr. D. Carlson Urbana, IL 61801
1	University of Dayton University of Dayton Research Institute ATTN: Mr. H. F. Swift Dayton, OH 45406		

DISTRIBUTION LIST

<u>No. of Copies</u>	<u>Organization</u>	<u>No. of Copies</u>	<u>Organization</u>
1	University of Iowa ATTN: Dr. K. Valanis Iowa City, IA 50010	1	Washington State University Department of Physics ATTN: Dr. G. E. Duvall Pullman, WA 99163
2	University of Kentucky Dept of Engineering Mechanics ATTN: Dr. M. Beatty Prof. P. Gillis Lexington, KY 40506	2	Yale University ATTN: Dr. B. Chu Dr. E. Onat 400 Temple Street New Haven, CT 96520
2	University of Maryland Dept of Mechanical Engineering ATTN: Prof. Y. Yang Dr. J. Dally College Park, MD 20742		<u>Aberdeen Proving Ground</u>  Marine Corps Ln Ofc Cdr, USATECOM ATTN: Mr. W. Pless Mr. S. Keithley Dir, USAMSAA ATTN: Dr. J. Sperrazza Mr. G. Zeller Mr. T. Nolan
1	University of Minnesota Dept of Engineering Mechanics ATTN: Dr. R. Fosdick Minneapolis, MN 55455		
4	University of Texas Dept of Engineering Mechanics ATTN: Dr. C. H. Yew Prof. Ripperger Prof. Bedford Dr. J. T. Oden Austin, TX 78712		
1	University of Washington Dept of Mechanical Engineering ATTN: Prof. J. Chalupnik Seattle, WA 98105		